

DIPLOMARBEIT

Hochaufgelöste korrelative Mikrosokopie anhand des Modellorganismus *Arabidopsis Thaliana*

zur Erlangung des akademischen Grades

Diplom-Ingenieurin

im Rahmen des Studiums

Biomedical Engineering

eingereicht von

Tamina May Laimer

Matrikelnummer 01026896

ausgeführt am Institut für Angewandte Physik
der Fakultät für Technische Physik der Technischen Universität Wien

Betreuung

Betreuer: Univ.Prof. Dipl.-Ing. Dr.techn. Gerhard Schütz
in Zusammenarbeit mit Dr. Andreas Walter, Bioimaging Austria - CMI

Wien, 13.02.2019

Tamina May Laimer

Gerhard Schütz

MASTER'S THESIS

**Towards Super-Resolution CLEM
Using The Model Organism
*Arabidopsis Thaliana***

to obtain the academic degree of

Master of Science

in the course of the study

Biomedical Engineering

by

Tamina May Laimer

Matriculation number 01026896

carried out at the Institute for Applied Physics
of the Vienna University of Technology

Supervision

Supervisor: Univ.Prof. Dipl.-Ing. Dr.techn. Gerhard Schütz
in cooperation with Dr. Andreas Walter, Bioimaging Austria - CMI

Vienna, 13.02.2019

Tamina May Laimer

Gerhard Schütz

Zusammenfassung

Korrelative Bildgebung ist eine Methode, bei der zwei oder mehr komplementäre Bildgebungsverfahren verwendet werden um Informationen über eine Probe zu sammeln. Dadurch kann ein ganzheitliches Bild der Probe erzeugt werden, in welchem die gesamte relevante Informations- und Auflösungs-spanne genutzt wird. Das Ziel dieses Projekts war, eine Methode zu entwickeln, die die Mikroskopiemethoden direct Stochastical Reconstruction Microscopy (dSTORM) und Transmissionselektronenmikroskopie (TEM) miteinander korreliert und genutzt werden kann, um Autophagie in Pflanzen zu erforschen. Autophagie ist ein essentieller Mechanismus, der in biologischen Zellen vorkommt und Teil der Qualitätskontrolle der Zelle ist. Sie gewährleistet das Entfernen von unerwünschten oder überschüssigen Makromolekülen, die der Zelle potentiell schaden könnten. Während des Prozesses werden diese Makromoleküle von neu gebildeten, doppelmembranigen Vesikeln verschlungen, welche Autophagosomen genannt werden. Autophagosomen sind durch das Protein ATG8 (engl. autophagy-related protein 8) gekennzeichnet, welches für die Bildung der autophagosomalen Membran benötigt wird. Der Hauptfokus dieses Projekts war die Entwicklung und Optimierung von Probenvorbereitungsprotokollen, um die Kompatibilität zwischen den verschiedenen Fluoreszenz- und Elektronenmikroskopiemethoden (dSTORM und TEM) zu gewährleisten, und einer Strategie, um dieselbe Stelle mit den zwei verschiedenen Methoden zu detektieren. Wir haben die Verteilung von einzelnen ATG8-Proteinen mit dSTORM visualisiert und die Ultrastruktur von isolierten Zellkernen mit Autophagosomen mit TEM aufgelöst.

Abstract

Correlative imaging is a method used to gather information about a specimen by applying two or more complementary modalities. This allows to span the entire information and resolution range of interest and create a holistic view of the sample. This project aimed at developing a method to study autophagy in plants by correlating direct Stochastic Optical Reconstruction Microscopy (dSTORM) and Transmission Electron Microscopy (TEM). Autophagy is an essential quality control mechanism that appears in biological cells. It ensures removal of unwanted or excess macromolecules that could otherwise cause harm to the cell. During this process, these macromolecules get engulfed by newly-formed double membrane vesicles termed autophagosomes. They are labeled by the autophagy-related protein 8 (ATG8) that is required for the formation of the autophagosomal membrane. The main focus of this project was the establishment and optimization of sample preparation protocols to ensure compatibility between fluorescence and electron microscopy techniques (dSTORM and TEM), and the identification of labeling strategies that allow to detect the same region of interest with the two different modalities. We visualized the distribution of ATG8 at a single-molecule level using dSTORM, and the ultrastructure of isolated nuclei with autophagosomes using TEM.

Acknowledgements

I would first like to express my gratitude to Andreas Walter for giving me the opportunity to work for this project as part of Bioimaging Austria - CMI and to learn so many new things while working with various people from different research groups. He was truly supportive and inspired me with his enthusiasm for correlative imaging. I would also like to thank the experts who were involved in this project: Yasin Dagdas and Christian Löffke from Dagdas Group, who were pushing forward the project from the biological point of view and gave me insights in plant biology and autophagy, the Biophysics group, especially Benedikt Rossboth and Mario Brameshuber, who were helping me with my super-resolution experiments, the entire EM Facility, who provided me support with everything related to electron microscopy and more. I am very grateful that I worked with Alina Psenicny, without whom this entire journey would not have been the same. Finally, I would like to express my profound gratitude to my parents who have supported me throughout the years of study. This accomplishment would not have been possible without them.

Contents

1	Introduction	4
1.1	Motivation	4
1.2	Project Goals	5
1.3	Outline	6
2	Theory	7
2.1	Autophagy	7
2.2	Correlative Imaging	9
2.3	Microscopy Methods	11
2.3.1	Fluorescence Microscopy	12
2.3.1.1	Confocal Microscopy	14
2.3.2	Super-resolution Microscopy	15
2.3.2.1	dSTORM	15
2.3.3	Electron Microscopy	17
2.3.3.1	Transmission Electron Microscopy	18
2.4	Sample Preparation	19
2.4.1	Immunolabeling	19
2.4.2	Chemical Fixation	21
2.4.3	High Pressure Freezing	22
2.5	Correlative Light and Electron Microscopy	23
2.6	Image Registration	25
3	Methods & Material	27
3.1	Sample Material	28
3.2	Confocal Microscopy & dSTORM	30
3.2.1	Antibody Labeling	30
3.2.2	Sample Preparation	31
3.2.2.1	General Protocol	31
3.2.2.2	Adapted Sample Preparation	32
3.2.3	Data Acquisition	32
3.2.4	Post-Processing	33

3.3	Transmission Electron Microscopy	33
3.3.1	Sample Preparation	33
3.3.1.1	General Protocol	33
3.3.1.2	Adapted Sample Preparation	35
3.3.2	Data Aquisition	36
3.4	Correlation	36
3.4.1	Sample Preparation	36
3.4.1.1	General Protocol	36
3.4.1.2	Fiducial Markers	39
3.4.2	Data Aquisition	39
3.4.3	Image Registration	40
4	Results	43
4.1	Confocal Microscopy & dSTORM	43
4.1.1	Antibody Concentration	43
4.1.2	Confocal Microscopy	44
4.1.3	dSTORM	46
4.2	Transmission Electron Microscopy	49
4.3	Correlation	52
5	Discussion & Conclusion	56
A	ThunderSTORM Settings	58
B	References	60

List of Abbreviations

AFS	Automated Freeze Substitution device
ATG	Autophagy-related protein
BSA	Bovine Serum Albumin
CLEM	Correlative Light and Electron Microscopy
Col-0	Columbia
CT	X-ray Computed Tomography
dSTORM	direct Stochastic Optical Reconstruction Microscopy
EM	Electron Microscopy
FPALM	Fluorescence Photo-Activation Localization Microscopy
GA	Glutaraldehyde
GFP	Green Fluorescent Protein
HPF	High Pressure Freezing
MES	2-(N-morpholino)ethanesulfonic acid
MRI	Magnetic Resonance Imaging
MS	Murashige and Skoog medium
PALM	Photo-Activation Localization Microscopy
PBS	Phosphate Buffered Saline
PET	Positron Emission Tomography
PFA	Paraformaldehyde
PSF	Point Spread Function
SAD	Sum of Absolute Differences
SPECT	Single Photon Emission Tomography
SSD	Sum of Squared Differences
STED	Stimulated Emission Depletion
STORM	Stochastic Optical Reconstruction Microscopy
TBST	Tris-buffered Saline with Tween 20
UA	Uranyl Acetate

CHAPTER 1

Introduction

1.1 Motivation

Aristotle said that “the whole is greater than the sum of its parts.” While many people may know this quote in the context of team building, it is also very accurate in the biomedical context of bioimaging and microscopy. With many different modalities available, imaging has become an inherent part in biomedical research. In theory, one can choose the most suitable modality to answer a specific research question, but in reality, sometimes even the most suitable modality cannot access all the necessary information by itself. This inaccessibility of holistic information sparked the urgent need for correlative imaging. Correlative imaging is the combination of different modalities to yield information that cannot be obtained by one modality alone. Even though the concept has been around for almost 60 years, it has gained significantly more attention in the last 5 years, with more and more papers being released about new correlative imaging methods (see Figure 2.4A). Since correlative imaging methods open up the possibility to tackle so far inaccessible research questions, the development and implementation of new correlative methods is of utmost importance.

As the biological research question, we chose to study autophagy in the model plant *Arabidopsis thaliana*. Autophagy is a cellular process that is well studied in animals, whereas it is less well described in plants. It is not only of great interest to shed light onto a so far unknown field, but also are plants practical to use during method development.

This project was carried out for Bioimaging Austria - CMI as a collaboration of Vienna University of Technology, Vienna Biocenter Core Facilities and the Gregor Mendel Institute of Molecular Plant Biology.

1.2 Project Goals

The overall aim of this project was to develop a correlative workflow to study autophagy in the plant *Arabidopsis thaliana*. This workflow should include different microscopy methods:

- Light sheet microscopy to generate an atlas showing the emergence of autophagy in roots under varying stress conditions by visualizing ATG8 protein (see A. Psenicny's work [1])
- Super-resolution microscopy dSTORM to image the distribution of ATG8 in autophagosomes at a single-molecule level
- Transmission electron microscopy (TEM) to visualize the ultrastructural context underlying the previously detected ATG8

The aim of this thesis was to initiate and set up this project regarding the correlation of dSTORM and TEM. This included several sub-goals:

1. Establishment and optimization of sample preparation protocols for
 - (a) dSTORM
 - (b) TEM
 - (c) correlative dSTORM and TEM
2. Implementation of a program to align the acquired data

This should later on be used to visualize the distribution of ATG8 proteins to show how they are distributed and oriented on the autophagosomal membrane and shed some light on autophagy research.

1.3 Outline

The following thesis explains the theoretical background as well as the implemented methods. Chapter 2 gives an overview over the basic theory. First, the mechanism of autophagy is explained to give the reader relevant biological background. Different imaging modalities, which were used during this project, are introduced as well as the concept of correlative imaging. It is described how samples can be prepared for fluorescence and electron microscopy to clarify the difficulties that come along with correlative light and electron microscopy. In the end, it is explained how acquired images can be aligned by registration. In Chapter 3, the various methods are described, including sample preparation protocols and information about the data acquisition with the used modalities. Additionally, the implemented registration program is explained. Chapter 4 presents the results that were obtained. Finally, the thesis finishes with a discussion and a conclusion that summarizes the presented work including the difficulties, which were faced.

CHAPTER 2

Theory

2.1 Autophagy

During the life cycle of eukaryotic cells a considerable amount of waste, such as aged proteins and damaged organelles, accumulates within the cell. One of the major cellular processes to remove this biological waste from the cell is *autophagy* (from the Ancient Greek *autóphagos*, meaning “self-devouring”)[2, 3]. Nonselective autophagy is primarily known as a starvation response, whereas cells use selective autophagy for a variety of purposes, e.g. adaption to changing environmental/nutritional conditions and to eliminate damaged organelles. As a consequence, defects in selective autophagy are associated with a range of pathophysiologies in humans, including certain types of neurodegenerative diseases. There are various types of autophagy, including the two main types termed *macroautophagy* and *microautophagy*. The characteristic feature of macroautophagy is the formation of a compartment, which expands into a double-membrane that surrounds the cell component that needs to be degraded. In the case of microautophagy, the sequestration event takes place directly at the limiting membrane of the lysosome/vacuole [4].

In this thesis we will focus on *macroautophagy* and refer to it as *autophagy* in terms of simplicity.

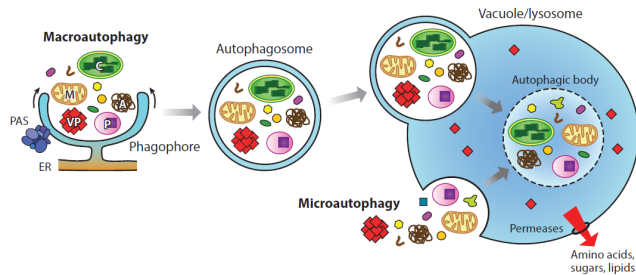


Figure 2.1: Morphological steps of microautophagy and macroautophagy [5].

Autophagy starts with the assembly of a membrane termed *phagophore*, which is believed to be created from the endoplasmic reticulum. The phagophore engulfs cytosolic components and closes to form a double membrane vesicle termed *autophagosome*. Autophagosomes get transported via the cytoplasm to the vacuole (in plants), where the outer membrane of the autophagosomes fuse with the tonoplast to release the internal cargo as an autophagic body into the vacuole. The cargo gets degraded and the resulting products get transported back into the cytosol for reuse [5].

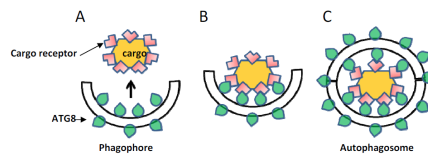


Figure 2.2: Mediation of selective autophagy [2].

Coordinated action of more than 30 core proteins known as *autophagy-related proteins (ATG)* are involved in the execution of autophagy. Selective autophagy is regulated through specific interactions of autophagy cargo receptors and ATG8 proteins. Autophagy cargo receptors define which molecules are targeted for degradation. Since ATG8 is one of the key molecular components, it is often used as a marker for autophagy [6]. In the plant *Arabidopsis thaliana* there are 9 different ATG8 proteins (ATG8A-ATG8I) [7].

However, the exact process of how a cell component is targeted for sequestration and segregated from other parts of the cell is one of the major questions in selective autophagy research [4]. Additionally, it is still not known, how the ATG8 are distributed and oriented on the autophagosomal membrane, and how this affects the targeting of the cargo. High resolution visualization of the ATG8 is needed to gain more insights into the autophagy machinery.

2.2 Correlative Imaging

Nowadays, there is a broad range of imaging modalities available. They have different specificities and limitations concerning individual mechanisms of tissue contrast, specific sensitivity, spatial and temporal resolution, as well as concerning the visualization of diverse biological processes [8]. While single modalities are adequate for some research questions, there are cases in which they are not sufficient to reveal all the information of interest. That is why nowadays it is of high interest to combine two or more modalities on the same sample by *correlative imaging*, which allows to integrate the strengths of the individual modalities and to overcome their weaknesses. Correlative imaging aims at spanning the entire information space of interest by gathering complementary information about structure, function, dynamics and chemical composition [9].

Examples for well-established correlative imaging methods are the combination of Positron Emission Tomography (PET) or Single Photon Emission Computed Tomography (SPECT) with X-Ray Computed Tomography (CT) or Magnetic Resonance Imaging (MRI). Whereas PET and SPECT images provide functional information, CT and MRI provide anatomical information, which is lacking in nuclear imaging modalities [8]. A study by Antoch et al. (2004), which assess the accuracy of combined PET/CT, showed that tumor staging with PET/CT is significantly more accurate than CT alone, PET alone, and side-by-side PET and CT. Out of 260 patients 84% were correctly staged with PET/CT, 76% when PET and CT were evaluated side by side, 63% with CT alone, 64% with PET alone [10, 11]. This shows how the combination of different modalities can be used to improve accuracy, when a single modality is not accurate enough.

However, another important aim of correlative imaging is to gather information across scales, meaning to span the entire resolution range of interest [9]. By cleverly combining different modalities, it is possible to study samples not only at varying magnitudes of resolution but also at varying magnitudes of penetration depth. Figure 2.3 shows the relationship between spatial resolution and penetration depth. Clinical imaging methods such as PET, CT, MR and ultrasound have rather poor spatial resolution, but high penetration depth compared to microscopy methods, which have higher resolution, but can penetrate tissue only in the μm range.

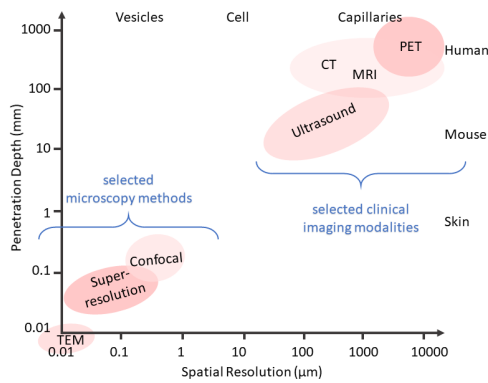


Figure 2.3: Penetration depth as a dependence of spatial resolution, adapted from Sarah Bohndiek, University of Cambridge.

Correlative imaging is becoming increasingly popular in biomedical research. At first, only few peer-reviewed papers dealt with correlative imaging each year, but the continuously improving hard- and software and substantial progress in method development led to a large increase in correlative imaging.

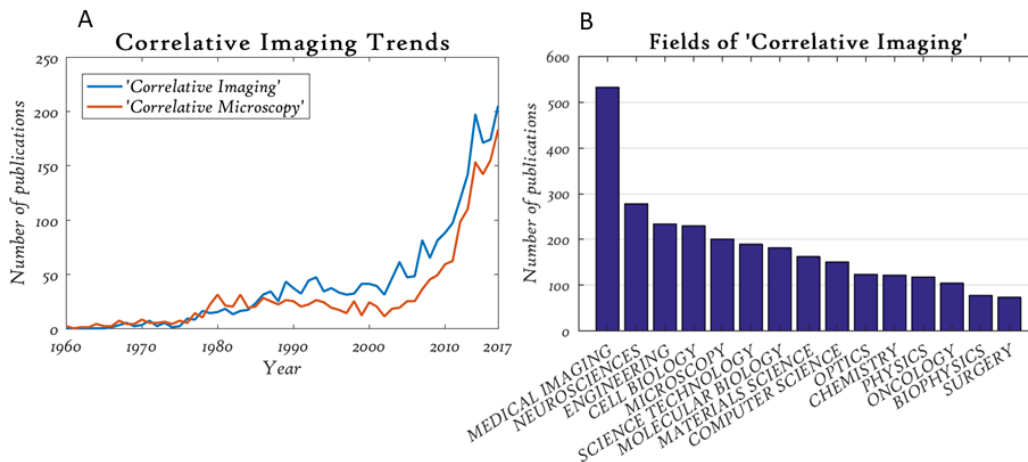


Figure 2.4: A: Number of publications in PubMed published every year, containing ‘Correlative Imaging’ and ‘Correlative Microscopy’, data from [12]. B: Research areas with highest number of publications regarding ‘Correlative Imaging’, data from [13].

2.3 Microscopy Methods

In 1873, Ernst Abbe observed that the image of a point object in a microscope is given by a diffraction pattern, which results from interference of the light rays in the image plane. This diffraction pattern is called *point spread function (PSF)* or *Airy function*. When highly magnified, it can be seen that this function consists of a large central peak, which contains 84% of the light from the point source and is surrounded by smaller peaks of decreasing amplitude. The width of the central peak, called *Airy disk*, is determined by the wavelength and the aperture angle of the lens, and is given by equation

$$d_{xy} = 0.61\lambda/\text{NA} \quad (2.1)$$

where λ is the wavelength of the transmitted (fluorescent) light and NA is the numerical aperture with $\text{NA} = n \cdot \sin \theta$, where n is the refractive index of the medium between the lens and the specimen and θ the half angle over which the objective can collect light coming from a nearby object. This equation also describes the so-called *Rayleigh criterion* for the resolution of two close point objects in the xy-plane. It states that two adjacent object points can be resolved when the maximum of one disk overlaps with the first minimum of the other disk. Closer objects are unresolved [14].

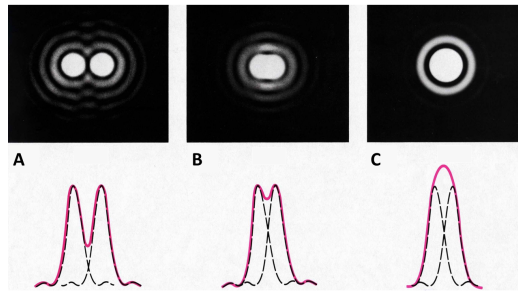


Figure 2.5: Rayleigh criterion for two point objects. A: Two points that are clearly resolved. B: Two points at Rayleigh limit that can be barely resolved. C: Two points that cannot be resolved anymore [15].

The thickness of the Airy disk along the z-axis is given by

$$d_z = \lambda n/\text{NA}^2 \quad (2.2)$$

which shows that axial resolution is even worse than resolution in the xy-plane [14]. Under ideal conditions, a lateral resolution of about 200 nm and

an axial resolution of about 500 nm can be achieved [16].

This massive limitation was not overcome until a century after Abbe described the diffraction limit. In 1957, the confocal microscope was invented, which could achieve slightly better resolution than regular light microscopes. Few years earlier, electron microscopy, which is an alternative concept using electrons instead of light, was born. Electron microscopy could achieve resolution that was never reached before, but at the cost of extensive sample preparation. Today, there are different super-resolution microscopy methods available that can achieve nanometer precision with the use of fluorescence microscopes [17].

2.3.1 Fluorescence Microscopy

Fluorescence microscopy uses either special dyes called *fluorophores* or fluorescent proteins to specifically label non-fluorescent subcellular structures in a specimen to make them visible [14]. The development of methods to conjugate proteins to fluorophores in the early 1940s and the cloning of the *green fluorescent protein (GFP)* in the early 1990s, which permits to label proteins of interest specifically by genetic encoding, have dramatically raised popularity of fluorescence microscopy [17]. Nowadays, there are many different fluorophores and GFP variants available [18]. Due to the great specificity and relative ease of use, fluorescence microscopy is until now the most frequently used mode of light microscopy in biomedical research [14].

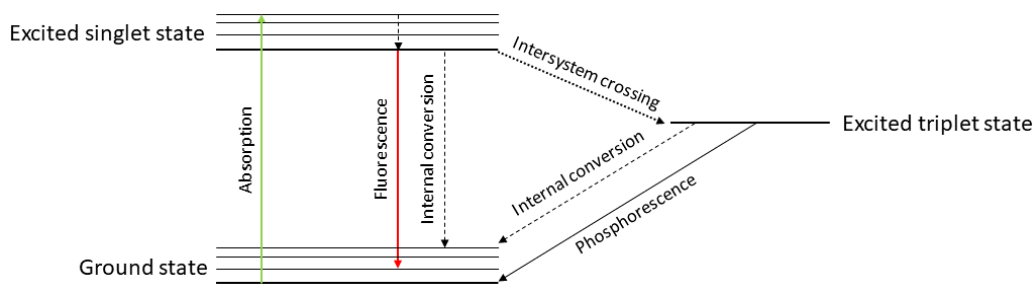


Figure 2.6: Jablonski diagram, adapted from [14].

The principle of fluorescence can be described with a so-called *Jablonski diagram* (see Figure 2.6), which shows different energy states as horizontal lines. When an electron absorbs a photon of appropriate wavelength, it gets excited from the ground state to a singlet state. Naturally, the electron almost immediately goes back to the ground state. There are three pathways how

this can be achieved: it can emit a photon (fluorescence emission), it can release vibrational energy as heat (internal conversion) or it can transfer to an excited triplet state (intersystem crossing). When an electron is in the triplet state, it can return to the ground state either by internal conversion or by emission of phosphorescence [14].

In fluorescence microscopy, the excitation of the fluorophores of interest is achieved by an excitation light at a wavelength that will excite the fluorophores and is usually provided by a laser. When stimulated by light, fluorophores emit light with a higher wavelength. This light can then be detected by the photodetector. Both the excitation light and the resultant emission fluorescence are usually passed through a dichroic mirror. The dichroic mirror reflects the incoming, higher-energy (but shorter wavelength) excitation light, but allows the lower-energy (higher wavelength) fluorescent light to pass through to the light detector [14, 18].

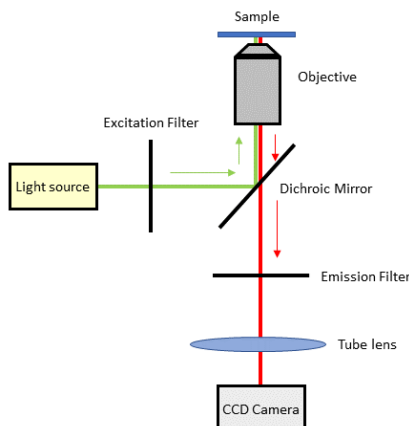


Figure 2.7: Fluorescence microscopy set-up, adapted from Gerhard Schütz, Technische Universität Wien.

Even though fluorescence microscopy is a powerful tool, it also has limitations. The most severe limitation is the phenomenon of *photobleaching*, which is the light-induced destruction of fluorophores. When fluorophores are in an excited state, they are more likely to react with other molecules, e.g. oxygen. It is thought that triplet states strongly contribute to photobleaching, due to their longer lifetimes and stronger reactivity [19]. When making measurements over time, every effort should be made to minimize photobleaching over the course of the acquisition, e.g. by minimizing exposure times or excitation intensity [20].

2.3.1.1 Confocal Microscopy

Confocal laser scanning microscopy, also known as confocal microscopy, was developed in 1955 by Marvin Minsky. Compared with conventional microscopes, they create sharper and better contrasted images with less background. Additionally, they have the ability to image a stack of confocal image planes that can be used to create 3D images. Confocal microscopy can also be used for real-time microscopy to track dynamic events. Due to these advantages, fluorescence confocal microscopes have become the workhorse for biological research [18].

Working principle

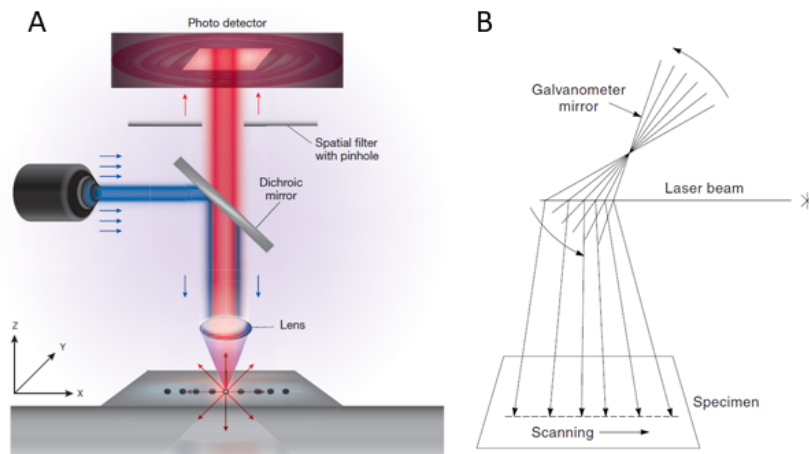


Figure 2.8: A: Simplified view of confocal microscopy [18]. B: Scanning principle with galvanometer-driven-mirrors [14].

Confocal microscopes have a similar set-up to regular fluorescence microscopes, but with an additional pinhole aperture. The specimen is illuminated with a focused laser scanning beam (point scanning), which is moved across the object by galvanometer-driven mirrors. The coordinated motions of the mirrors generate a raster pattern on the specimen: one mirror controls scanning along the x-axis, the other one along the y-axis [14]. The principal component of this microscope is the use of a small pinhole aperture in a screen that allows only the light emitting from the desired focal spot to pass through, while any light originating from outside of the focal plane is blocked. The pinhole is placed in a conjugate focal plane to the specimen. On the other side of the pinhole there is a photodetector to detect the confocal light [18].

Even though the use of a pinhole is very effective to block out-of-focus detection, it does not inhibit out-of-focus excitation. This means that photobleaching of fluorescent probes and phototoxicity of live samples are not reduced compared to conventional fluorescence microscopes [18].

Resolution

The spatial resolution d for two fluorescent point objects is given by

$$d_{xy} \approx 0.4\lambda/\text{NA} \quad (2.3)$$

$$d_z \approx 1.4\lambda n/\text{NA}^2 \quad (2.4)$$

The use of a constricted pinhole increases resolution in the x,y plane, but decreases resolution in axial direction by a factor of 1.4 [14, 21].

2.3.2 Super-resolution Microscopy

In 1994, Stefan Hell et al. developed stimulated emission depletion (STED) microscopy [22] and became pioneers in the field of *super-resolution microscopy*. STED microscopy was the first illumination-based super-resolution microscopy method and uses a donut-shaped depletion laser to reduce the size of the PSF of the excitation laser and, as a consequence, improves the image resolution. In 2006, three research labs came up with single-molecule based approaches: Betzig called it photo-activation localization microscopy (PALM) [23], Hess called it fluorescence photo-activation localization microscopy (FPALM) [24] and Zhuang called it *stochastic optical reconstruction microscopy (STORM)* [25, 26]. Even though the implementation of the methods vary, they all use the same principle: instead of activating all fluorophores at once, only a small subset is activated at a time. The central position of the single fluorophores can then be determined with nanometer precision. Afterwards, the activated fluorophores are photobleached or deactivated and the next subset is activated. To be able to generate an extensive image, it is necessary to repeat the cycle many thousand times, which reduces the image acquisition speed, but localization precision can be improved to 10-55 nm [26]. This opened entirely new possibilities in the study of single molecules.

2.3.2.1 dSTORM

The first implementation of STORM used two different fluorophores called *activator* and *reporter dye*, which were conjugated onto an antibody. The reporter dye is excited by the imaging laser to generate the fluorescence that

forms the final image. The activator dye is used to stochastically activate a small subset of the reporter dye, which is maintained in a non-fluorescent state by an imaging buffer. When stimulated with an activation laser, the activator dye can cause a neighboring reporter dye to become fluorescent [27]. In 2008, Heilemann et al. described an approach which does not rely on the use of activator and reporter dyes in a specific ratio and specific distance and referred to it as '*direct*' *STORM* (*dSTORM*) [28]. With *dSTORM*, a single laser can be used during acquisition which continuously illuminates the sample, and no activation laser is needed [27].

Working principle

When preparing the specimen for the experiment, *photoswitchable* fluorophores are attached to the structure of interest. Usually, approximately once every 1000 excitations a molecule transits to a dark triplet state. The lifetime of the triplet state is naturally only a few microseconds and is therefore invisible. By addition of a special *STORM imaging buffer* to the specimen, the fluorophores can reversibly switch between fluorescent and dark states, when excited with a laser. The imaging buffer reduces molecular oxygen and by this increases the lifetime of the triplet state to milliseconds, making the reversible on/off transitions visible. The majority of the photoswitchable fluorophores is turned to a dark state by an intense laser light. During the experiment, only a small subset of single fluorophores is switched on by a lower-intensity excitation laser and read out. This procedure of photoactivation and readout is repeated to record thousands of frames. Afterwards, the reconstruction of a super-resolution image is achieved by localizing the single activations in every frame [29, 30].

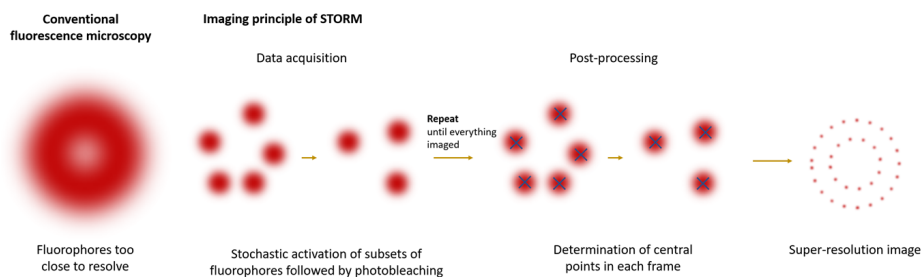


Figure 2.9: The working principle of STORM.

Resolution

The spatial resolution in *dSTORM* is determined by the localization precision Δx that in turn is dependent on many parameters. If the background noise

is negligibly low, a simple estimation can be given by

$$\langle(\Delta x)^2\rangle = \frac{s^2}{N} \quad (2.5)$$

where s is the standard deviation of the fitted Gaussian distribution and N is the number of the collected photons. This means that brighter fluorophores result in better localization precision [31]. Labeling density also plays a role, since the final dSTORM image is a point-by-point reconstruction. If there are not sufficiently dense fluorescent labels, the resolution of the final image will be reduced. Another factor is the size of the probes. Antibodies with a size of 10-15 nm are often used to fluorescently label the specimen, which can result in a distance of up to 30 nm to the target molecule in the case of the use of primary and secondary antibody. Alternative labeling strategies with nanobodies can reduce this distance to 4-6 nm. In fixed cells, lateral resolution of 10 nm and axial resolution of 20 nm was achieved [27].

2.3.3 Electron Microscopy

Electron microscopy uses accelerated electrons, which have both particle and wave characteristics, to observe structures in the nanometer range. Electrons can have wavelengths that are thousands of times shorter than those of visible light (about 2 pm at an accelerating voltage of 200 kV compared to 200 nm in light microscopes), resulting in much higher resolution compared to conventional fluorescence microscopy. The relationship between electron wavelength λ and kinetic energy of the electrons eV is given by

$$\lambda = \frac{h}{\left[2m_0eV \left(1 + \frac{eV}{2m_0c^2}\right)\right]^{1/2}} \quad (2.6)$$

with h the Planck's constant, m_0 the rest mass of the electron and c the speed of light in vacuum. Equation 2.6 states that the electron wavelength can be decreased by increasing the acceleration voltage of the microscope. This means that resolution can be dramatically increased by increasing the acceleration voltage. It also includes relativistic effects that significantly appear above 100 kV [32].

In general, there are two main types of electron microscopy: *Scanning Electron Microscopy (SEM)* is used to obtain topographical images of the sample surface by scanning the object with an electron beam in a raster scan pattern. *Transmission Electron Microscopy (TEM)* is used to image ultra-thin sections of a specimen by transmitting an electron beam through the very thin (ideally <80 nm) sections [33].

2.3.3.1 Transmission Electron Microscopy

In TEM, samples need sophisticated preparation:

1. Biological samples have very low contrast, which needs to be enhanced by introducing heavy metals, such as osmium tetroxide.
2. Samples need to be fixed and completely dry to be stable in the vacuum inside the microscope.
3. In contrast to visible light microscopy methods, electron microscopes use ionizing radiation, resulting in strong interaction with matter including absorption and inelastic scattering. Therefore, samples need to be very thin, which is achieved by resin embedding followed by sectioning in an ultramicrotome. Usually, sections of the readily prepared sample are collected on a holey copper grid, which is then inserted into the microscope via a sample holder [34].

Working principle

The principal components of electron microscopes are electromagnetic lenses that focus the electron beam. Electrons are emitted by an electron gun operated with acceleration voltages of 50 kV-1 MV (80-300 kV for biological samples). After passing the condenser lenses and the condenser aperture, the electron beam passes the specimen and enters the objective lens, followed by the objective aperture. After some intermediate steps, which are not shown in Figure 2.10, the beam gets broadened by the projector system. The magnified image can then be seen on the screen or on a connected camera [34].

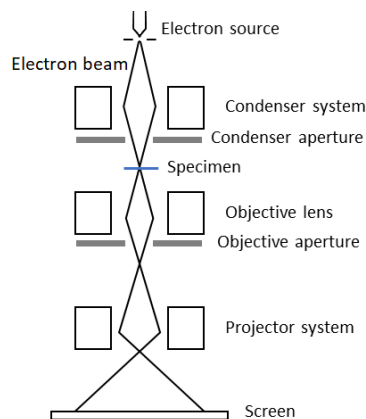


Figure 2.10: Schematics of the working principle of TEM, adapted from [34].

Resolution

As seen in equation 2.6, higher voltages equal smaller wavelengths resulting in higher resolution. At the same time, higher voltages result in a decreased

cross section for all forms of scattering, which has important implications for electron-beam damage in sensitive samples. Additionally, lens aberrations prohibited resolution below 0.1 nm (1 Å) for a long time [32]. In biological samples imaged at room temperature (after chemical fixation), resolution is additionally limited by preparation artifacts. The principle of cryo-EM, using cryogenic temperatures for observing structures in a near-native state, is pushing forward resolution, and structures as small as 2 Å have been resolved in biological samples. Due to radiation damage and low contrast of biomolecules, this is still far above the theoretical possible, diffraction-limited resolution of a few picometer [35]. In material science a resolution of 0.39 Å was reached by Muller in 2018 by using an ultra sensitive detector and a special method for reconstructing data [36].

2.4 Sample Preparation

Biological samples need to be thoroughly prepared to yield accurate and representative results. The detailed sample preparation depends on the microscopy method as well as the structure of interest. One common procedure to label structures of interest for fluorescence microscopy is *immunolabeling*, which uses antibodies to target specific proteins. Another common procedure, which is used for fluorescence microscopy and TEM, is *fixation*. The goal of fixation is to maintain cells, cellular formations or tissue in their current state and stop all cellular processes, which would otherwise occur during further processing, e.g. degradation [37]. In general, there are two ways how a sample can be fixed, either by *chemical* or *physical fixation*. The following sections cover these steps in general. The protocols that were used during the project are listed in Chapter 3.

2.4.1 Immunolabeling

There are many antibodies commercially available, which can be used to target almost every protein. *Antibodies* are glycoproteins and bind specific antigens. Depending on the antibody class, they consist of one or more Y-shaped units. Each Y consists of two identical heavy chains and two identical light chains. The upper part of the Y is the so-called variable region, which binds specifically to an epitope of the antigen, whereas the lower part is the so-called constant region, which determines the class of the antibody (see Figure 2.12) [38]. There are two ways how immunolabeling can be performed:

either by *direct* or *indirect immunofluorescence*. In direct immunofluorescence, the primary antibody is conjugated with a fluorophore, which makes the structure of interest visible under the microscope. In indirect immunofluorescence, primary antibodies are first used to target the structure of interest. Afterwards, secondary antibodies, conjugated with a fluorophore, are used to label the first antibody. This method is more time consuming, but is generally more flexible due to greater variety of commercially available secondary antibodies [37, 39].

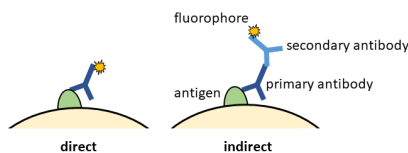


Figure 2.11: Direct and indirect immunofluorescence.

One novel class of antibodies are so-called *nanobodies* or nanotraps (e.g. GFP-Trap). Nanobodies are single-domain antibody fragments and were developed from camelidae (e.g. alpacas). Camelidae antibodies consist of heavy chains only with a single variable domain. These single variable domains were isolated and can now be used to specifically bind to an epitope of an antigen. Whereas conventional antibodies have an atomic mass of around 150 kDA, nanobodies are significantly smaller with an atomic mass of 15 kDA [40, 41].

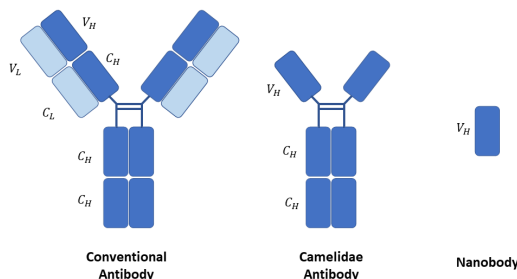


Figure 2.12: Regions of different antibodies (variable region V, constant region C, light chain L, heavy chain H).

However, independent of which method and antibody is used, a typical immunolabeling workflow consists of the following steps: after cells are fixed, membranes are permeabilized with detergents (e.g. Triton X-100) to enable antibodies to enter the cells. Blocking is performed with bovine serum albumin (BSA) for example to reduce unspecific binding with non-target structures. Then, the sample is incubated with the primary antibody and, if the indirect method was chosen, with a secondary antibody [37].

2.4.2 Chemical Fixation

Chemical fixation is a fixation method which is based on the use of chemical reagents. It is the most common approach to fix biological samples. There are different reagents which are often used and have slightly different effects.

- *Formaldehyde* is a classical fixing agent and has various complex chemical properties. It can penetrate rapidly into tissue due to its small size. Formaldehyde cross-links proteins via its free amino groups. Even though the initial binding to proteins is quite fast, the formation of (partially reversible) methylene bridges occurs more slowly. In fluorescence microscopy, when using immunolabeling, 4% formaldehyde for 10 minutes at room temperature is often used for various cell lines and antigens [37, 42]. Most commercially available formaldehydes are nowadays prepared from paraformaldehyde (PFA)[43].
- *Glutaraldehyde (GA)* is a fixative, which is especially useful for ultra-structural studies. It is more efficient in cross-linking proteins and inhibiting enzyme activity than formaldehyde. The disadvantage is that GA has a slower rate of penetration than formaldehyde, therefore they are often used in combination to yield satisfying results. Additionally, GA is not suitable for immunofluorescence studies, due to its high level of autofluorescence [42].
- *Acetone* denatures proteins, causes precipitation of proteins and dehydration of tissues. It can be used in immunofluorescence studies and, when using cold acetone fixation, it can be used to maintain enzyme activity. Acetone can also be used for dehydration during epoxy embedding [42].
- *Osmium tetroxide* is an electron dense fixing agent, which is often used to increase contrast in electron microscopy. It reacts with unsaturated lipids. During the cross-linking process, dark brown to black compounds are formed. It is mainly used as a secondary fixing agent after aldehyde because it can not fix all proteins when used alone [42].

Plant material can be challenging to fix. It has been observed that vacuoles often rupture prior to fixation and therefore alter the cellular organization. When chemical fixation is used, one needs to be aware that there is no ideal fixative. Thus, compromises have to be made when selecting a protocol. Additionally, the quality of fixation is dependent on many variables, e.g. rate of penetration, concentration of fixing agents, length of fixation and temperature [42].

2.4.3 High Pressure Freezing

Physical fixation procedures can overcome deficiencies of chemical fixation, but are technically more challenging. A physical fixation method that is frequently used to fix bigger samples (up to 600 μm thick) is *High Pressure Freezing (HPF)*. HPF uses rapid freezing to fix the sample. The formation of ice crystals needs to be avoided to yield samples without morphological damage. The growth of ice crystals as well as the form of ice are dependent on the cooling rate. High cooling rates are needed to vitrify the water in a sample. In 1975, Kanno et al. observed that the nucleation of ice crystals is dependent on both temperature and pressure [45] (see Figure 2.13). This means that by applying a high pressure of 2100 bar directly before freezing, the freezing properties of waters are changed and, as a consequence, lower cooling rates are required to vitrify samples [42, 44].

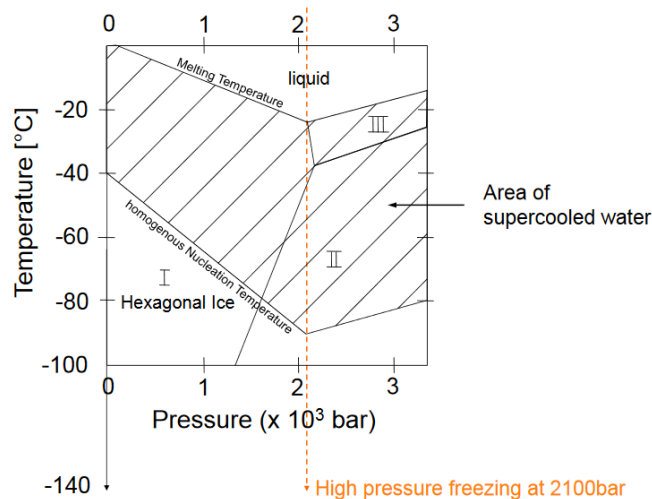


Figure 2.13: Phase diagram showing the states of water in dependence of temperature and pressure. I, II, III are different phases of ice [46].

After freezing, frozen samples undergo *freeze substitution*. Freeze substitution uses organic solvents (e.g. acetone) with or without fixing agents (e.g. uranyl acetate (UA)) to replace the vitrified water within the sample at low temperatures. Afterwards the sample is either infiltrated at low temperatures with an embedding medium such as Lowicryl HM20 or the sample is slowly warmed up to room temperature and embedded into an epoxy resin. Freeze substitution is not necessary, if the sample is observed under a cryo-microscope. This preserves the sample close to the native state, but requires a lot of experience [42, 44].

2.5 Correlative Light and Electron Microscopy

The concept of correlative microscopy has been around for almost 50 years, but several challenges still restrict the everyday application: Sample preparations for different microscopy methods are often not compatible with each other and require adaption to ensure compatibility. Furthermore, it is necessary to find the same region of interest with different modalities using sophisticated software, and special hardware is needed to transfer the sample between the different microscope platforms. One example of correlative microscopy that is gaining more and more popularity is *Correlative Light and Electron Microscopy (CLEM)*. Fluorescence microscopy methods allow researchers to identify and study specifically labeled structures (live or fixed), but without information about the unlabeled surrounding. For studying the ultrastructure of a sample, electron microscopy is still the method of choice, but identifying structures of interest only by means of morphology can be challenging and live cell imaging is not possible. By combining both methods, structures of interest can be identified with a higher degree of confidence and in context of their surroundings [47].

In principle, there are two ways how CLEM can be performed:

1. *Sequential*: Samples are prepared and studied under the fluorescence microscope, followed by EM-related sample preparation and observation under the electron microscope. This way sample preparation for both modalities can be individually optimized and is not influenced by each other. The disadvantage is that observed structures can change between the modalities; in live cell imaging due to the movement of the cells, but even in fixed samples due to the following sample preparation [48, 49]. This change, commonly shrinkage, can be nonisotropic and difficult to correct for, which is especially disadvantageous if very small structures need to be correlated with nanometer precision. The sequential approach is particularly suitable to observe dynamic events in a larger field of view under the fluorescence microscope with subsequent fixation and high-resolution imaging under the electron microscope [48].

2. *Integrated*: Resin blocks or ultra-thin sections are prepared, labeled and fixed such that they can be imaged both by fluorescence microscopy and EM without intermediate sample preparation steps. This results in the most accurate correlation, since the exact same sample is studied using both modalities. The disadvantage is that sample preparation protocols need to be mod-

ified to ensure compatibility. To get high quality fluorescence images, it is necessary to preserve as much fluorescence as possible, but at the same time, the ultrastructure should not be harmed to get best possible EM images. In EM, a combination of PFA and GA is often used for chemical fixation. It has been shown that GA quenches fluorescence and at the same time introduces background fluorescence. However, reducing GA can result in worse preservation of the ultrastructure. Another component that is known for significantly reducing fluorescence is osmium, which is regularly used during chemical fixation to additionally fix and stain samples. There have been different approaches to circumvent this problem. One is to reduce the osmium concentration to a level that still preserves membrane fixation and contrast without quenching fluorescence [48, 49]. Another approach is to use HPF instead of chemical fixation with further UA staining after fluorescence imaging to increase contrast in electron microscopy [49]. Independent of which of these two approaches is used, the proper choice of resin is also important. The most popular resin in EM is the epoxy resin Epon, which gives hard samples, but most proteins are denaturated. In integrated CLEM, the most widely applied resins are methacrylate resins Lowicryl and LR white. These hydrophilic resins give less contrast and softer blocks, and it has been claimed that it is difficult to cut acrylic resins thinner than 70 nm. However, they (in contrast to epoxy resin) preserve fluorescence. Additionally, resin sections must be relatively thick (70-100 nm) to produce sufficient fluorescence signal [48, 50].

In both the sequential and integrated way, it is necessary to find the same region of interest in the microscope and to accurately register the acquired images. Commercially available finder grids can be used to locate the previously observed area and for a coarse alignment of the images. For more accurate alignment *fiducial markers*, which are visible in both modalities, can be used [49].

Traditional CLEM has a significant mismatch in resolution, but with the novel super-resolution microscopy methods, CLEM can now provide better matched scales between modalities [49]. When using an integrated approach to correlate STORM and EM, the wrong choice of resin does not only reduce fluorescence, but additionally prevents the photoswitching properties of the fluorophores by cross-linking the molecules and altering the environment. Therefore the right choice of resin is crucial for super-resolution CLEM [48, 51].

2.6 Image Registration

Correlative imaging can only reach its full potential when the data obtained from separate images are combined. This integration step consists of the spatial alignment of the images followed by image fusion to generate a combined view of the object. The alignment of the images, but sometimes even the whole process including image fusion, is termed *registration* [52]. The aim of registration is to find a transformation that maps one image onto another image, so that corresponding voxels match [53]. To be able to develop a registration program, it is necessary to know what kind of registration methods exist and how they can be applied. In the following, different types of transformations are described.

Registration distinguishes between *monomodal* and *multimodal* registration. Monomodal registration uses images acquired with the same modality, which can be useful e.g. to compare images taken at different time points. Multimodal registration uses images generated with different modalities, as it is usually done in correlative imaging, to get complementary information about the object. While monomodal registration is, due to their high degree of similarity between the images, quite straightforward, it is more complicated in the multimodal case [52].

Registration methods can be divided into *extrinsic* and *intrinsic* methods. Extrinsic methods are based on objects, which are artificially introduced into the sample (fiducial markers). As fiducial markers are - independent of the modality - well detectable, they significantly simplify the registration process. Intrinsic methods are based on information given by the specimen. This information can be a set of landmarks (i.e. eye-catching points) or a similarity measure computed from the grey values of the image. The use of fiducial markers or landmarks can be additionally categorized into *point-based* registration. Methods based on similarity measures do not only use a set of points but the entire information of an image, which makes them most flexible but at the same time computationally expensive [52, 54]. For both monomodal and multimodal registration, there are many similarity measures available. Similarity measures that assume a functional relationship between intensities (and are used for monomodal registration) are sum of squared differences (SSD), sum of absolute differences (SAD) and correlation coefficient. Popular measures that assume a statistical relationship (and are used for multimodal registration) are joint entropy, mutual information and nor-

malized mutual information [53].

An important aspect that strongly influences the complexity of a registration is the required coordinate transformation. A transformation is called *rigid* if the distance between any two object points is preserved, meaning only rotation and translation are allowed. If scaling and shear is additionally allowed, a transformation is called *affine*. Affine transformations preserve parallelism, thus map a line onto a line. A *projective* transformation is like an affine transformation that does not preserve parallelism of lines. *Elastic* transformations map lines onto curves [52, 54]. The applicability of a registration process depends on the required transformation. For example, landmark-based registrations are mostly used for rigid or affine transformation, because landmarks usually need to be thoroughly identified by a user and the number of landmarks defines which transformations can be applied (complex transformation need more points than simple ones) [52].

Another important aspect is the user interaction during registration. A registration algorithm can be *automatic*, *semi-automatic* or *interactive*. Whereas an automatic algorithm only needs the image data and optionally additional information about the image acquisition, an interactive registration solely assists the user, who does the registration himself. In semi-automatic methods, the user needs to either initialize the algorithm (e.g. selecting fiducial markers) or accept/reject a suggested registration. Even though it is often desired to have fully automated algorithms, there is often a trade-off between minimal interaction and robustness, speed and accuracy, which can make automation difficult [52].

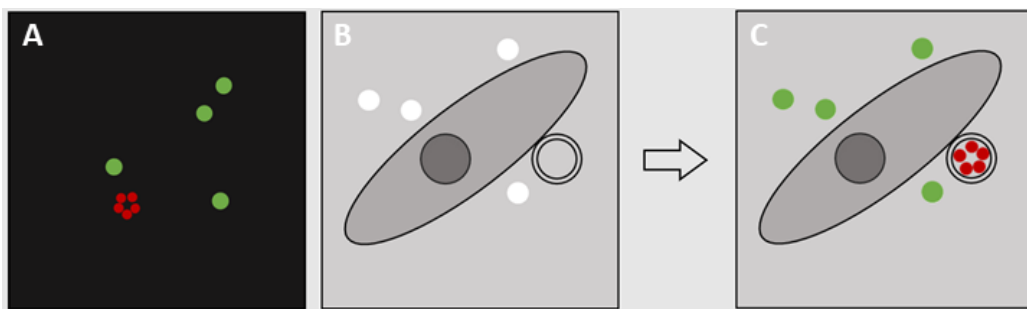


Figure 2.14: Illustration of a multimodal registration with fiducial markers (rigid transformation). A: Fluorescence image. B: TEM image. C: Registered image.

CHAPTER 3

Methods & Material

To correlate dSTORM with TEM, the following strategy was applied. First of all it was necessary to establish a best standard for the model organism *Arabidopsis thaliana* for each imaging modality. To study autophagosomes in super-resolution, isolated nuclei were chosen as a suitable specimen, due to observations that autophagosomes are often attached to nuclei. By this, it was expected to increase the number of autophagosomes in the sample, which should make it easier to detect autophagosomes under the microscope. DNA damage was induced to additionally increase autophagosome formation.

To optimize the dSTORM protocol, labeling strategies were needed to conjugate fluorophores to the ATG8 protein. This includes selecting the linker type (antibody or nanobody) and determining the right concentration to get a satisfying signal-to-noise ratio. The quality of the sample preparation was additionally checked under the confocal microscope, due to easy handling, accessibility and the possibility to record three dimensional volumes.

For TEM, it was necessary to set up a working protocol that provides good ultrastructure preservation. Chemical fixation followed by epoxy resin embedding has been chosen, because it has led to good results in Arabidopsis roots in the past and was easier to perform than HPF.

The sample preparation additionally needed to be optimized in terms of nucleus isolation, which caused unexpected challenges. This included using buffers with different Triton X-100 concentration, to find a preparation that did not heavily damage the ultrastructure. This was checked under the confocal microscope with a membrane stain and under the TEM.

At last, we aimed at setting up a working protocol for super-resolution CLEM. To get the most accurate correlation, an integrated approach has been chosen. To preserve fluorescence, HPF was applied after immunolabeling isolated nuclei, and Lowicryl resin HM20 was used for embedding.

Strategies to find the same region with both modalities were needed. This included the choice of suitable finder grids and fiducial markers. During this stage, a commercial CLEM microscope, which is designed for fluorescence imaging of grids, was used to search the sections for fluorescence. Along the way, a program for point-based registration of correlative images was implemented in MATLAB.

The following sections cover this process in more detail.

3.1 Sample Material

During this project, different mutants of the plant *Arabidopsis thaliana* were used. We started with Columbia (Col-0) to study ATG8-A. Later on, we additionally used a transgenic line that expresses GFP at ATG8-E. A mutant expressing KAKU-tRFP was used in between to study the nuclear membrane after nucleus isolation.

Cultivation of plants was similar for all types: plant seeds were sterilized with ethanol and distributed under a laminar flow hood on plates with Murashige and Skoog medium (MS) and 1/2 sucrose concentration buffered with 2-(N-morpholino) ethane sulfonic acid (MES), shortened '1/2 MS + MES'. The sealed plates were stored at least for 2 days in a 4°C chamber. Afterwards, they were transferred into a growth chamber for 7-12 days with a 16 h daylight cycle, a room temperature of 21°C and 60% humidity.

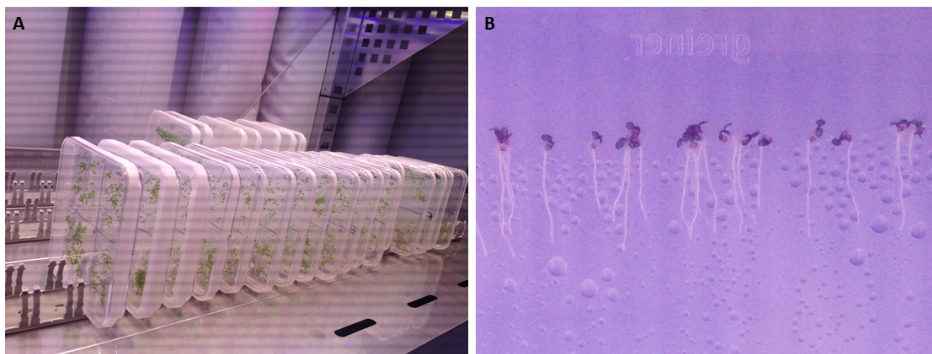


Figure 3.1: A: Plates arranged in growth chamber. B: 7 day old *Arabidopsis thaliana* on a plate with 1/2 MS + MES.

The following protocol was used in slightly modified versions to yield isolated nuclei for further sample preparation for confocal, dSTORM, TEM and the correlative workflow.

1. DNA damage & pre-fixation

1. Around 10 seedlings were put into 100 μ l Bleomycin in 50 ml liquid 1/2 MS + MES for 1-2 hours (in the dark) to induce DNA damage.
2. Afterwards, seedlings were washed with liquid 1/2 MS + MES.
3. The plants were fixed in 2 ml ice-cold 4% formaldehyde in Tris Buffer for 20 min to fix and preserve the plant tissue.
4. The seedlings were washed two times with ice-cold Tris Buffer for 10 min.

2. Isolation of nuclei & purification

1. For isolation of the nuclei the plant material was chopped with a razor blade in LB01 lysis buffer in a small Petri dish on ice to a fine suspension.
2. The suspension was filtered through a Corning Cell Strainer with 40 μ m nylon mesh.
3. The sample was spun down at 4°C for 5 min with 500 g and washed with LB01 lysis buffer until the pellet became white or light green, indicating that the chloroplasts have been removed from the sample.

The following buffers were used to prepare the samples.

- Tris buffer: 10 mM Tris-HCl, pH 7.5, 10 mM Na₂-EDTA, 100 mM NaCl
- LB01 lysis buffer: 15 mM Tris-HCl, pH 7.5, 2 mM Na₂-EDTA, 0.5 mM spermine · 4 HCl, 80 mM KCl, 20 mM NaCl, 0.1% Triton X-100

3.2 Confocal Microscopy & dSTORM

3.2.1 Antibody Labeling

Immunolabeling was used to label the ATG8-A protein in isolated nuclei of Col-0. This was done by directly conjugating fluorophores to the primary antibody. This reduces the distance of the fluorophore to the structure of interest by half compared to labeling with primary and secondary antibody. A polyclonal, rabbit Anti-APG8A antibody (ab77003, abcam) was conjugated to the fluorescent dye Alexa Fluor 647 (life technologies) via N-hydroxysuccinimide (NHS) ester labeling. This labeling procedure is based on the reaction of NHS ester-activated crosslinkers and labeling compounds of the fluorophore with primary amines of the antibody. In physiological to slightly alkaline conditions (pH 7.2 to 9) both components react to yield stable amide bonds. The reaction releases NHS (see Figure 3.2)[55].

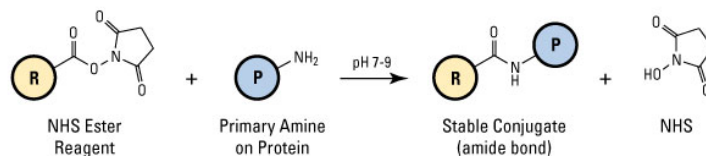


Figure 3.2: NHS ester reaction scheme for chemical conjugation to a primary amine [55].

Labeling with 5-fold molar excess of dye in phosphate buffered saline (PBS) with 10% NaHCO_3 for 30 minutes at room temperature and consequent purification with a Zeba Spin Desalting Column yielded an average degree of labeling (DOL) of 3.4, meaning that there are approximately 3.4 fluorophores per antibody. The DOL was determined photometrically using the microplate reader Synergy H1 by BioTek and the associated data analysis software Gen5.

The same procedure with 4-fold molar excess of dye in PBS with 10% NaHCO_3 was used to directly conjugate Alexa Fluor 647 to the GFP-Trap (chromotek). The GFP-Trap binds to the GFP in the GFP-ATG8-E line and is even smaller than the previously used antibody. Through this, a DOL of 1.4 was achieved.

3.2.2 Sample Preparation

The sample preparation protocol for fluorescence microscopy was developed based on a protocol by H. Wang, which is an adapted version of [56] and was additionally modified for the use with dSTORM in this project.

3.2.2.1 General Protocol

1. Immunolabeling

1. For immuno-detection of the ATG8-A (or ATG8-E) protein, the sample was first incubated in 1% BSA in TBST for 30 min to reduce unspecific binding of the antibody (or GFP-trap).
2. The sample was then washed with TBST for 5 min with 500 g.
3. The primary antibody (or GFP-trap) labeled with Alexa Fluor 647 was added to the sample in 1% BSA and incubated for 30 min at room temperature. An antibody (or GFP-trap) concentration of 200 $\mu\text{g/ml}$ was used (see 4.1.1 for further information).

2a. Further preparation for confocal microscopy

1. After washing with TBST, the sample was pipetted onto #1 microscopic slides and immediately postfixed with 4% formaldehyde in TBST at room temperature for 30 min.
2. The sample was again rinsed with TBST.
3. The cover slip was mounted in Vectashield with DAPI for chromatin detection onto an object slide and sealed with nail polish.

2b. Further preparation for dSTORM

1. After washing with TBST, the sample was pipetted onto #1 microscopic slide preassembled on a 8-well-chamber and immediately post-fixed with 4% formaldehyde in TBST at room temperature for 30 min.
2. The sample was again rinsed with TBST.
3. Before image acquisition for dSTORM, a switching buffer was added to the specimen to enable the photoswitching of the fluorophores.

The following buffers were used to prepare the samples.

- TBST: Tris-buffered saline with 0.5% tween
- STORM switching buffer: PBS (pH 7.4), containing oxygen scavenger (0.5 mg/ml glucose oxidase, 40 mg/ml catalase, 10% glucose) and 50 mM Cysteamine (based on the switching buffer used in [28])

3.2.2.2 Adapted Sample Preparation

- To find a suitable antibody (or nanobody) concentration, samples with varying antibody concentration have been prepared according to 3.2.2.1.
- To examine how Triton X-100 affects fluorescence labeling efficiency, GFP-ATG8-E line plants were prepared according to 3.2.2.1. A control, where nucleus isolation was done in LB01 lysis buffer without Triton X-100 was prepared.
- To see the affect of Triton X-100 on the membranes, KAKU-tRFP plants were prepared according to 3.2.2.1 with nucleus isolation in LB01 lysis buffer containing
 - 0.1% Triton X-100
 - 0.05% Triton X-100
 - no Triton X-100

3.2.3 Data Aquisition

Confocal Microscopy

The microscope used for confocal imaging was a LSM780 Axio Observer (inverted) with an incubator from Zeiss. For imaging the distribution of ATG8-A and ATG8-E, a Plan-Apochromat 63x/1.40 oil objective was used. For excitation of DAPI, a laser diode with wavelength of 405 nm and for excitation of Alexa Fluor 647, a HeNe laser with wavelength of 633 nm was used.

dSTORM

The microscope used for dSTORM imaging was an inverted Zeiss Axiovert 200 with a 640 nm diode laser (iBeam smart 640, Topica), which was led to the microscope via multiple mirrors. A Plan-Apochromat 100x/1.46 oil objective was used. The emission light was collected by an EMCCD camera. To control the laser shutter, AOM and the camera, an in-house programmed

LabVIEW package was used. The fluorophores were bleached by applying the unattenuated red laser through various planes for several seconds. In general, between 10000 and 20000 frames were recorded to get one super-resolution image.

3.2.4 Post-Processing

All images were post-processed with ImageJ [57]. Post-processing of the dSTORM data consisted of two steps. To increase the localization precision, static background - i.e. low frequency signals - were removed from the raw data with an in-house programmed Python script [58]. The script makes a Fourier transform of every pixelstack and removes 80% of the lowest frequency signals. By this, only the blinking fluorophores, that contribute to the reconstructed image, remain and the localization of the fluorophores in the focal plane is improved. For the fitting process, the ImageJ plugin ThunderSTORM was used [59]. The detailed settings are listed in Appendix A.

3.3 Transmission Electron Microscopy

3.3.1 Sample Preparation

A sample preparation protocol for Arabidopsis roots was provided by N. Fellner and was adapted for isolated nuclei. For TEM it was necessary to use a high amount of plants to get a visible pellet that can later on be trimmed. Therefore, plant material of 2-3 plates was used.

3.3.1.1 General Protocol

1. Fixation

1. The liquid was replaced by a fixative consisting of 2% GA and 2% PFA in 0.1 M Sörensen phosphate buffer over night at 4 °C.
2. The following day, the sample was washed three times with 0.1 M Sörensen phosphate buffer on a shaker for 5-10 min each.
3. To additionally fix and stain lipids, the sample was stored for 40 min in 2% osmium tetroxide in 0.1 M Sörensen phosphate buffer on ice.

4. The sample was then washed three times with the same buffer on a shaker for 5-10 min on ice.

2. Dehydration

The sample was gradually dehydrated with increasing acetone steps, each 10 min on ice.

- 40% acetone
- 60% acetone
- 80% acetone
- 90% acetone
- twice 100% acetone

3. Infiltration & embedding

The sample was gradually infiltrated with a mixture of acetone and Epon on a rotator (or shaker, if the sample was embedded in agarose).

- 2/3 100% acetone and 1/3 Epon for 2 hours
- 1/2 100% acetone and 1/2 Epon for 2 hours
- 1/3 100% acetone and 2/3 Epon overnight
- pure resin in desiccator for at least 2 hours
- pure resin for polymerization (48 h at 60 °C)

4. Trimming & Sectioning

1. The hardened sample was trimmed on a Leica EM Trim (Leica Microsystems) to a block face that was approximately 1 mm×1 mm in size (or smaller) and had at least two parallel edges.
2. The trimmed sample was then transferred into a Leica UCT ultramicrotome (Leica Microsystems). After aligning the block face of the sample to the knife edge of the ultramicrotome, the boat of the diamond knife was filled with double-distilled water and 70 nm sections were cut. The floating sections were then collected with 100 mesh grids with Formvar coating.

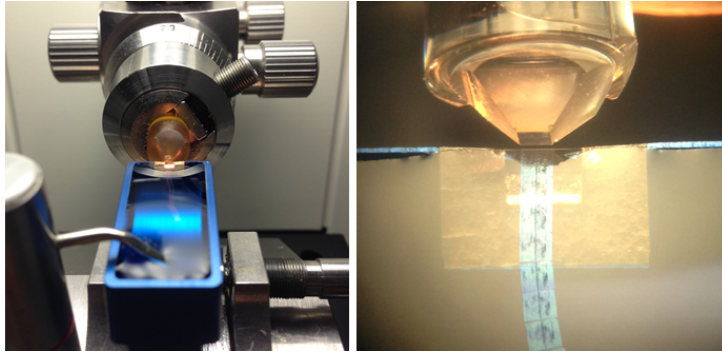


Figure 3.3: Sectioning with an ultramicrotome.

5. Post-Staining

To improve contrast, sections were post-stained with Reynold's lead citrate and 2% UA. After micro-centrifuging both agents in separate tubes for 10 min at maximal speed, grids were placed section-side-down on droplets of UA for 10 min. The grids were covered with a petri dish wrapped in aluminum foil to protect them from light. They were then rinsed with double-distilled water, dried with filter paper and placed section-side-down on droplets of Reynold's lead citrate, which were beforehand surrounded by sodium hydroxide pellets and covered with a petri dish. After 5 min, grids were again rinsed with double-distilled water and excess solution was removed with filter paper.

The following buffer was used to prepare the samples.

- 0.1 M Sörensen phosphate buffer

3.3.1.2 Adapted Sample Preparation

- Even though sample preparation started with a lot of plants, it was observed that consecutive exchange of buffers lead to a decreasing amount of isolated nuclei. Sometimes the effect was so severe, that the sample could not be seen during trimming and thus was accidentally trimmed away. To improve handling, the sample was embedded in 2% agarose before osmium tetroxide was used. When agarose was used, infiltration steps were extended.
- In order to improve ultrastructure preservation, different approaches were tried to properly fix the sample (see 4.9). Additionally, purification of the sample was skipped to get a bigger sample volume.

- To see the affect of Triton X-100 on the membranes, plants were prepared according to 3.3.1.1 with nucleus isolation in LB01 lysis buffer without Triton X-100.

3.3.2 Data Aquisition

The microscope used for TEM imaging was a 100 kV TEM FEI Morgagni 268D with a 11 megapixel CCD camera (Morada from Olympus-SIS). The microscope itself has a Tungsten filament emitter and is used at 80 kV. The microscope was operated via the Morgagni software (version 3.0) and image recording was done with the iTEM software (version 5.0).

3.4 Correlation

3.4.1 Sample Preparation

The correlative sample preparation protocol is a modified combination of the previously described protocols. As described in 2.5, there are in general two ways how fluorescence can be preserved in an integrated workflow: either by using chemical fixation with reduced GA and osmium tetroxide concentration or by applying HPF, which is a more technical approach. HPF has been chosen, due to the expectation that this approach preserves the ultrastructure of the sample better than chemical fixation. It was aimed to preserve fluorescence by embedding the sample into Lowicryl HM20 instead of epoxy resin. As in TEM, a high amount of plants was used to prepare the sample.

3.4.1.1 General Protocol

1. Immunolabeling

1. For immuno-detection of the ATG8-A (or ATG8-E) protein, the sample was first incubated in 1% BSA in TBST for 30 min to reduce unspecific binding of the antibody (or GFP-trap).
2. The sample was then washed with TBST for 5 min with 500 g.
3. The primary antibody (or GFP-trap) labeled with Alexa Fluor 647 was added to the sample in 1% BSA and incubated for 30 min at room

temperature. An antibody (or GFP-trap) concentration of 200 µg/ml was used (see 4.1.1 for further information).

4. The sample was then washed three times with TBST for 5 min each with 500 g.

The following steps (HPF, freeze substitution, infiltration and embedding) were done in close collaboration with A. Psenicny [1] and mainly follow the protocol by Reipert et al. [60]. For HPF, a Leica EMPact with a flat specimen holder system was used. After HPF, all steps were done in an automated freeze substitution device (AFS) by Leica.

2. High Pressure Freezing

1. The excessive liquid was removed and the sample was mixed 1:1 with 20% BSA.
2. A small amount of the sample was pipetted onto a flat gold-plated specimen carrier, placed on the specimen holder.
3. The carrier (containing the sample) was attached to a carrier holder and to a loading device, then transferred into the HPF system and was rapidly frozen with approximately 1950-2045 bar.
4. The frozen sample was released into a liquid nitrogen bath, where it was detached from the loading device and the carrier holder using pre-cooled tools.
5. After repeating this procedure several times, the carriers (including the samples) were moved into the pre-cooled AFS.

3. Freeze Substitution

1. The carriers were moved into a freeze substitution medium consisting of 0.5% UA in 100% acetone, which was previously pre-cooled to -90°C.
2. Freeze substitution was performed for at least 2 days at -90°C. Afterwards the temperature was raised up to -40°C, at the rate of 2°C/h.
3. After this temperature was reached, the samples were washed three times with pure acetone.

4. Infiltration & Lowicryl embedding

1. The samples were gradually infiltrated with a mixture of acetone and Lowicryl resin HM20.

- 2/3 100% acetone and 1/3 HM20 for 1 hour
 - 1/2 100% acetone and 1/2 HM20 for 2 hours
 - 1/3 100% acetone and 2/3 HM20 for 1 hour
 - Pure HM20 for 1 hour
2. Before starting polymerization, samples were moved into PCR cups attached to a holder, called spider cover. A drop of HM20 was applied to the lids of the PCR cups. The sample carriers were then moved, sample-side-up, with pre-cooled tweezers onto the lids. The tubes of the PCR cups were attached to the lids, filled with HM20 and mounted on the spider cover.
 3. The UV light was placed on top of the AFS and the samples were polymerized for 24 h at -40°C . The spider cover has the advantage that, by reflection of the UV light, the sample can be polymerized from all sides.

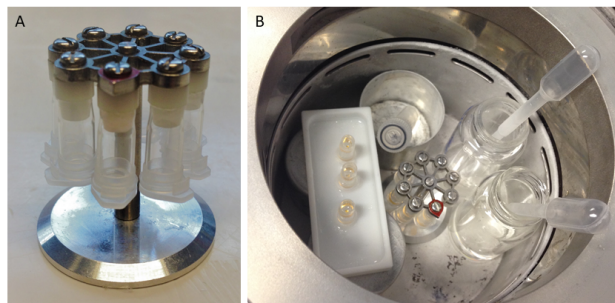


Figure 3.4: A: PCR cups on spider cover. B: Transfer of infiltrated samples into PCR cups for polymerization inside AFS.

4. After polymerization, the samples were gradually warmed up to room temperature. If not used immediately, samples were stored in the dark to preserve fluorescence.

5. Trimming & Sectioning

1. The PCR cup and the sample carrier were removed with a razor blade and the embedded samples were kept. The samples were trimmed similar to the TEM samples (see 3.3.1.1).
2. 150 nm sections were cut and collected with 400 mesh copper finder grids with and without Formvar coating. Fluorescence imaging was done within 1 day after sectioning, because fluorescence is known to vanish faster in sections than in resin blocks (see [61]).

3.4.1.2 Fiducial Markers

The use of fiducial markers is essential to get an accurate correlation. The fiducial markers need to be visible under fluorescence microscopes and under the TEM. Different fluorescently labeled microspheres from Invitrogen (listed in Table 3.1) have been tested to find suitable candidates.

Name	Size (μm)	Spectrum
FluoSpheres carboxylate-modified microspheres	0.02	yellow-green
FluoSpheres streptavidin-labeled microspheres	0.04	yellow-green
TetraSpeck microspheres	0.1	blue/green/orange/dark red

Table 3.1: Properties of used fiducial markers, data from [62].

Microspheres were applied in different concentrations either directly on cover slips or on coated grids. Additionally, application on sections as described in [61] was tested. For this, microspheres were first sonicated for 5 min using a Branson 2510 sonicator. Grids were placed section-side-down onto a 15 μl drop of microspheres for 10 min. The liquid was removed with filter paper and washed three times with a drop of double-distilled water and subsequently dried with more filter paper.

3.4.2 Data Acquisition

dSTORM

The correlative workflow needs a special imaging set-up to enable dSTORM. For STORM it is essential, that the fluorophores get in contact with the imaging buffer, thus a sandwich assembly introduced by Kukulski et al. [61] was tested. A drop of imaging buffer was applied on circular cover slips. The grid was placed section-side-down on the imaging buffer. Vacuum grease was applied on the outer rim and the cover slip was carefully closed with another cover slip to prevent drying.

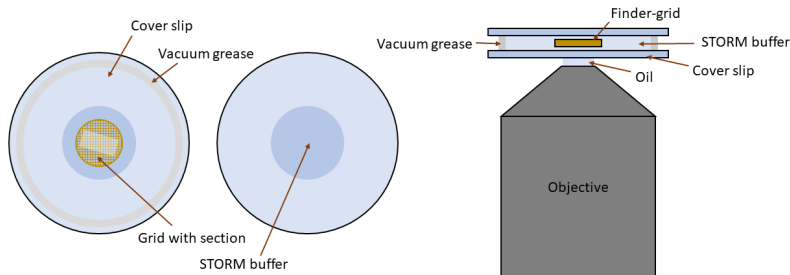


Figure 3.5: Set-up for dSTORM of sections on EM-grid.

CLEM

To further examine fluorescently labeled sections, a Leica EM Cryo-CLEM system was used. The CLEM microscope was equipped with a Plan-Apochromat 50x/0.9 cryo-objective and a sCMOS camera (Leica DFC9000). For fluorescence excitation a Leica DFC9000GT was used. The CLEM microscope was originally designed for imaging under cryo conditions, but was used at room temperature. The grid needs to be inserted into the microscope via a special transfer system before starting. In combination with the SerialEM software, the CLEM system is a powerful tool to automatically image the same region of interest with both modalities, by transferring the coordinate system from the CLEM microscope to the TEM. This was not compatible with the TEM device (100 kV TEM FEI Morgagni 268D) that was used for this project, but we could still benefit from the CLEM system. Image recording was done with the LAS X software. First, the grid was observed under the CLEM microscope. When a region of interest was found, a fast sketch of the grid position was made. The use of finder grids was important, because they contain letters and/or numbers that help orientation on the grid. The sample was transferred into the TEM and, with help of the sketch, the same region was located and imaged.

3.4.3 Image Registration

A function for point-based registration (using fiducial markers) was implemented in MATLAB [63]. Because fluorescence and TEM images are taken without sample preparation steps in between data acquisition with both modalities, the sample does not change, meaning that rotation and translation is sufficient. But since the field of view is not necessarily the same, additional scaling is necessary for a successful registration. The implemented function is semi-interactive and uses MATLAB's Image Processing Toolbox and the Computer Vision System Toolbox. The user selects at least three

fiducial markers in each image by clicking on them. A double-click adds the final point and closes the selection window. A rigid transformation gets calculated based on the iterative closest point algorithm using the coordinates of the selected fiducial markers. The images get scaled to the same size, resulting in an affine transformation. Additionally, the root-mean-squared error (RMSE) is calculated and returns the distance between the aligned points (x_i and y_i) as the euclidean distance [64].

$$\text{RMSE} = \sqrt{\sum_{i=1}^n \frac{(x_i - y_i)^2}{n}} \quad (3.1)$$

A RMSE of zero indicates a perfect fit, thus smaller values are desirable. It should be noted, that the RMSE is dependent on the absolute values and is not suitable to compare registrations of different datasets. In the end, the RMSE is displayed together with the two images after application of the transformation.

```

function [fixed , registered , rmse] = icp_registration (fixed , moving)
%input:
%fixed...reference image (e.g. TEM image)
%moving...image taken with different sensor (e.g. STORM image)

%output:
%images after registration
%root mean squared error (rmse) of euclidean distance between aligned points

%show input images before applying transformation
figure
imshowpair (fixed , moving , 'montage');
title ('Input_images');

%select pointcloud (fiducial markers) from both images
figure
imshow (moving);
[x1 , x2] = getpts;
m = size (x1);
movingPoints = [ones (m) , x1 , x2];
movingPoints = pointCloud (movingPoints);

figure
imshow (fixed);
[y1 , y2] = getpts;
n = size (y1);
fixedPoints = [ones (n) , y1 , y2];
fixedPoints = pointCloud (fixedPoints);

%get affine transformation from selected fiducial markers
[icp , ~ , rmse] = pcregrigid (movingPoints , fixedPoints);
T = icp .T (2:4 , 2:4);
tform = affine2d (T);

```

```

disp('RMSE: ');
disp(rmse);

%apply transformation
registered = imwarp(moving,tform);

%scale images to same size
registered = imresize(registered ,size(fixed));

%show images after applying transformation
figure
imshowpair(fixed ,registered , 'montage');
title('Registered_images');

```

Listing 3.1: MATLAB code for point-based registration.

```

fixed = 'TMV-2-modified.tif';
moving = 'TMV-7-modified.tif';

fixed = imread(fixed);
moving = imread(moving);

fixed = mat2gray(fixed);
moving = mat2gray(moving);

[fixed ,registered ,rmse] = icp_registration(fixed ,moving);

```

Listing 3.2: MATLAB code for applying point-based registration on two tif files.

Results

4.1 Confocal Microscopy & dSTORM

4.1.1 Antibody Concentration

We generated a binding curve showing the corresponding intensities for varying antibody concentrations to find the best antibody concentration. When working with low antibody concentrations, the intensity is low because only a fraction of antigens is labeled. At too high antibody concentrations, unspecific binding of the antibody might appear and the background increases [65]. To avoid both scenarios labeling should be done at saturation concentration. We used 4 different antibody concentrations: 0.4 $\mu\text{g/ml}$, 4 $\mu\text{g/ml}$, 40 $\mu\text{g/ml}$ and 400 $\mu\text{g/ml}$. For every concentration 6-9 nuclei were imaged using the same laser power in epi configuration. The mean signal intensity was calculated by subtracting the mean background intensity from the mean intensity inside the nuclei. The binding curve, shown in Figure 4.1, was approximated by the function

$$y = \frac{B_{max} \cdot x}{K_d + x} \quad \text{with } x \in [0, 400]$$

B_{max} is the maximum specific binding in the same units as y .

K_d is the equilibrium binding constant, in the same units as x [66].

Nonlinear regression was used to yield $B_{max} = 12647$ and $K_d = 99.96 \mu\text{g/ml}$. The value of K_d corresponds to the antibody concentration at which the antigens are half saturated [67].

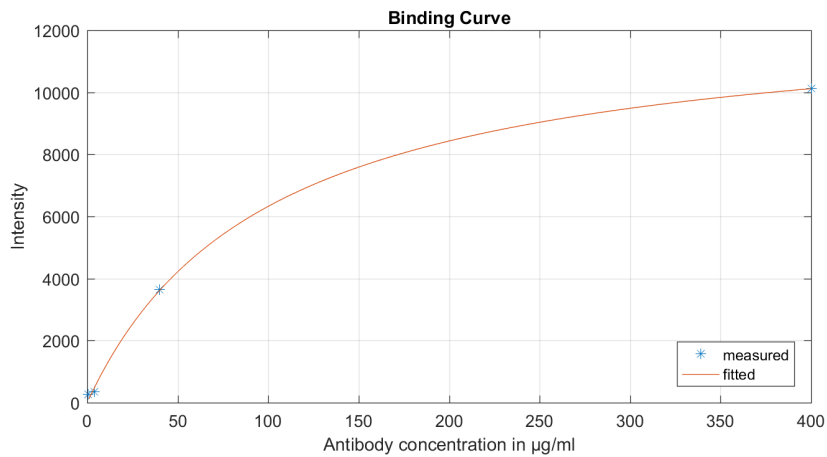


Figure 4.1: Binding curve showing corresponding intensities for four different antibody concentrations.

Even when evaluating only 4 different antibody concentrations, a tendency of the curve can be seen. For the subsequent experiments, we chose to work with an antibody concentration of 200 µg/ml. This value was also used for the GFP-trap to study ATG8-E.

4.1.2 Confocal Microscopy

Sample preparation according to the general protocol in 3.2.2.1 worked well for confocal microscopy. To get a good distribution of isolated nuclei and autophagosomes, it is important to use the right amount of plants and to stir the sample before applying it on a cover slip. Using too many plants or not stirring properly can result in irregular accumulations and agglutinated components, which is disadvantageous especially for single-molecule localization.

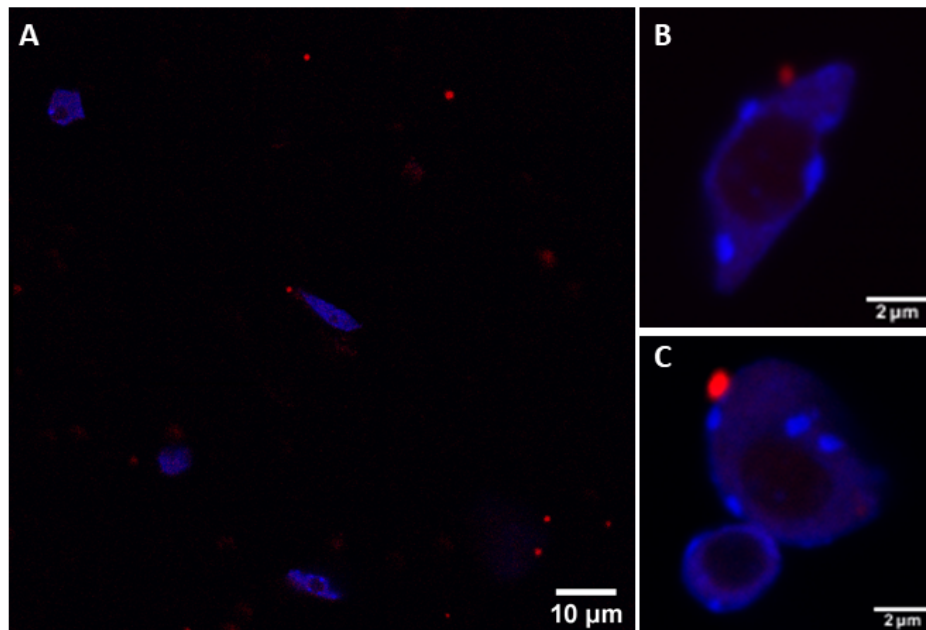


Figure 4.2: Isolated nuclei with autophagosomes. Blue color indicates chromatin, red color indicates ATG8-labeled autophagosomes. A: Overview image, ATG8-A labeled with Alexa Fluor 647. B, C: Close-up view of isolated nuclei with autophagosome, ATG8-E labeled with Alexa Fluor 647.

To prevent ultrastructural membrane damage by Triton X-100 as observed with TEM, sample preparation was additionally tested with nucleus isolation performed in LB01 lysis buffer without Triton X-100. It was confirmed that immunolabeling of ATG8-E was not successful without the essential permeabilization of the membranes, thus signals were barely detectable. It was necessary to find a compromise that allowed efficient immunolabeling and at the same time did not strongly damage membranes.

The quality of the nucleus isolation was further studied with KAKU-tRFP plants, which stained the nuclear envelope and thus made the effect of Triton X-100 on the membranes visible. The best results were archived with a concentration of 0.05% Triton X-100. Undamaged nuclei with intact chromatin organization were observed at that optimized Triton X-100 concentration. Even though the use of 0.1% Triton X-100 is common in fluorescence microscopy, it turned out to cause damage in this correlative project, because it resulted in holey and non-intact membranes, as visualized by TEM. Leaving out Triton X-100 is also not an option, because it resulted in worse quality and low fluorescence signals.

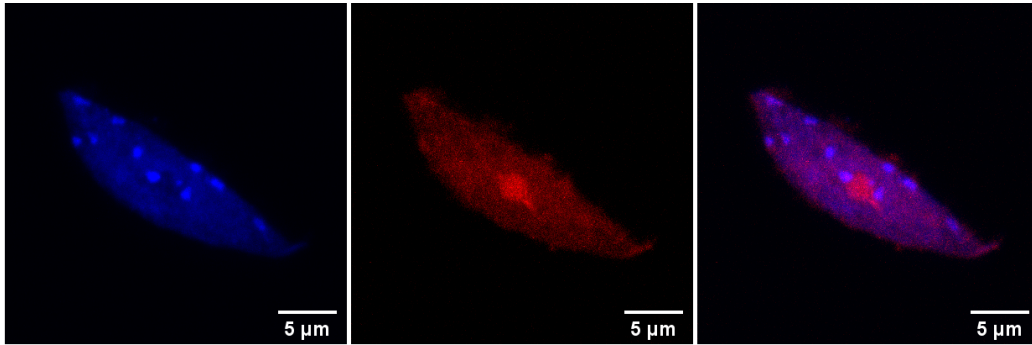


Figure 4.3: Maximum intensity projections of isolated nuclei permeabilized with 0.05% Triton X-100. Blue color indicates chromatin with DAPI staining, red color indicates the nuclear membrane labeled with tRFP. A: Blue channel. B: Red channel. C: Merged.

4.1.3 dSTORM

The first dSTORM samples were prepared using primary and secondary antibody according to H. Wang's 'Nuclei Immunostaining protocol for Arabidopsis', which was provided by Dagdas Group (GMI). After incubation with 1% BSA in a moist chamber at 37°C for 30 min, antigen detection was performed with a 1:200 dilution of primary antibody with 1% BSA overnight at 4°C. The secondary antibody labeled with Alexa Fluor 647 was applied in a 1:400 dilution with 1% BSA for 30 min at 37°C. By using this method, we observed very dense signals and a high background, especially when moving closer to the glass surface. By adapting the STORM imaging buffer, i.e. increasing the cysteamine concentration by a factor of 30, it was possible to prolong the dark state of the fluorophores. This improved the post-processing of the data, but modifications needed to be made to get optimized super-resolution images. The result of this first approach can be seen in Figure 4.4. ATG8-A is densely distributed throughout the nucleus and some background signals are visible.

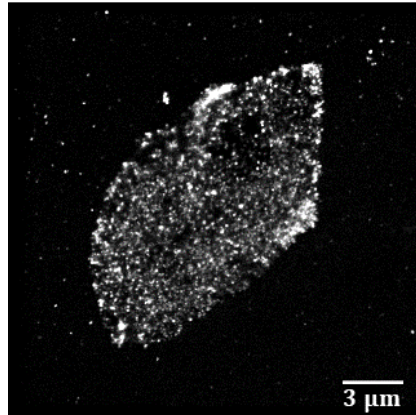


Figure 4.4: ATG8-A in an isolated nucleus labeled with Alexa Fluor 647 with the use of primary and secondary antibody and adapted STORM imaging buffer.

In the following, the labeling strategy was changed to direct immunofluorescence to decrease the distance from the fluorophore to the protein of interest. Images of ATG8-A labeled with an 1:5 dilution, i.e. a concentration of 320 $\mu\text{g}/\text{ml}$, of Alexa Fluor 647 on primary antibody with 1% BSA, can be seen in Figure 4.5. The signals were again very dense and the high background indicated unspecific binding. This showed the necessity to find an optimized antibody concentration (see 4.1.1) to avoid unspecific binding and to increase the signal-to-noise ratio.

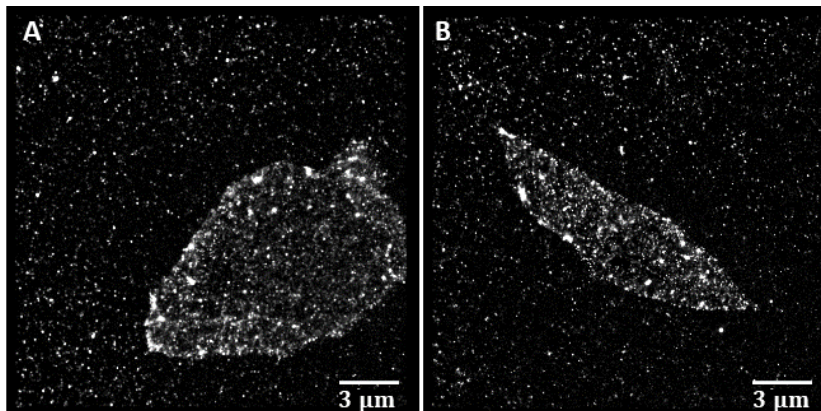


Figure 4.5: A, B: ATG8-A in an isolated nucleus labeled with Alexa Fluor 647 with the use of primary antibody.

After determining a suitable antibody concentration, samples were prepared with an antibody concentration of 200 $\mu\text{g}/\text{ml}$. Additionally, samples were incubated with the antibodies before positioning on a cover slip to decrease accumulations of fluorescently labeled antibodies on the glass surface. This

approach did not completely inhibit signals close to the glass surface, but an improved signal-to-noise ratio was achieved when going deeper into the sample. However, due to the background and the high density of the signals, the determination of the central position of the fluorophores was difficult. Removing low-frequency signals from the raw data significantly improved the fitting with a 2D Gaussian function (see Figure 4.6).

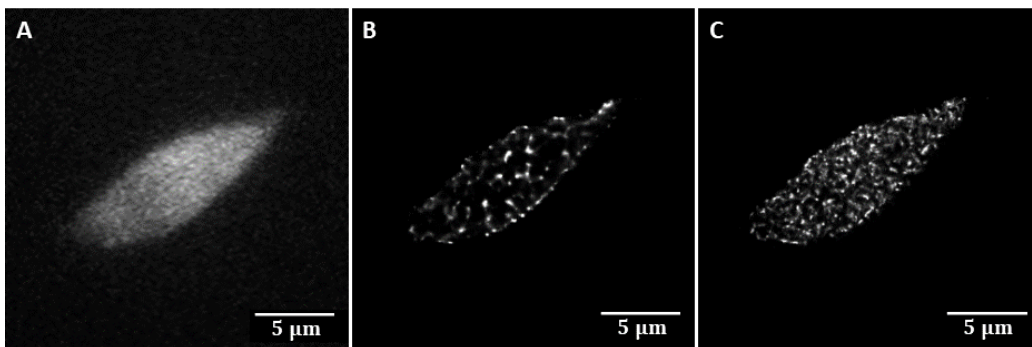


Figure 4.6: ATG8-A in an isolated nucleus. A: Image acquired before STORM imaging. B: STORM image. C: STORM image with improved post-processing.

The high amount of signals on the glass surface prevented data acquisition in total internal reflection (TIRF) mode and made it difficult to find single autophagosomes. A sample, where ATG8-E was labeled with Alexa Fluor 647 by a GFP-Trap, was prepared to see if the unspecific binding can be reduced by changing the linker type. This approach did indeed lead to better results. Ring like structures, which are characteristic for autophagosomes, could be detected. Low frequency signals were removed and ‘Multi-emitter fitting analysis’ was used in ThunderSTORM to improve the fitting procedure. However, even though the labeling quality was improved, the quality of the nuclei appeared to be rather poor which is indicated by a fuzzy contour of the nucleus in Figure 4.7A. This may be caused by the use of a non-optimized Triton X-100 concentration during nucleus isolation. For future dSTORM experiments, an adapted Triton X-100 concentration of 0.05% should be used.

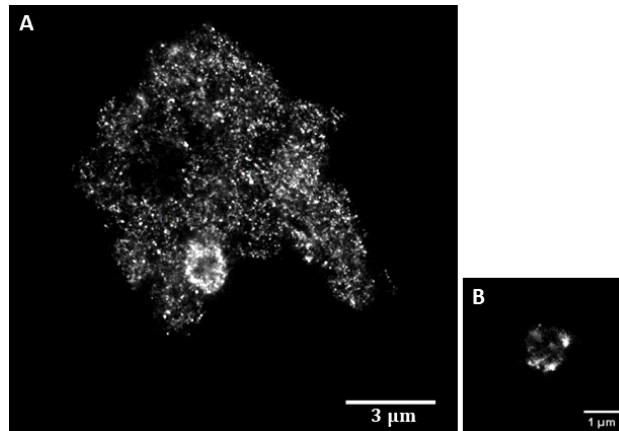


Figure 4.7: ATG8-E in isolated nuclei. A: Structures that appear to be two nuclei and an autophagosome. B: Potential autophagosome.

4.2 Transmission Electron Microscopy

The first attempt to prepare the sample for TEM included prefixation with 4% PFA for 20 min, followed by nucleus isolation in LB01 lysis buffer and subsequent purification. The sample was then fixed overnight at 4°C with 2% GA and prepared according to the general protocol.

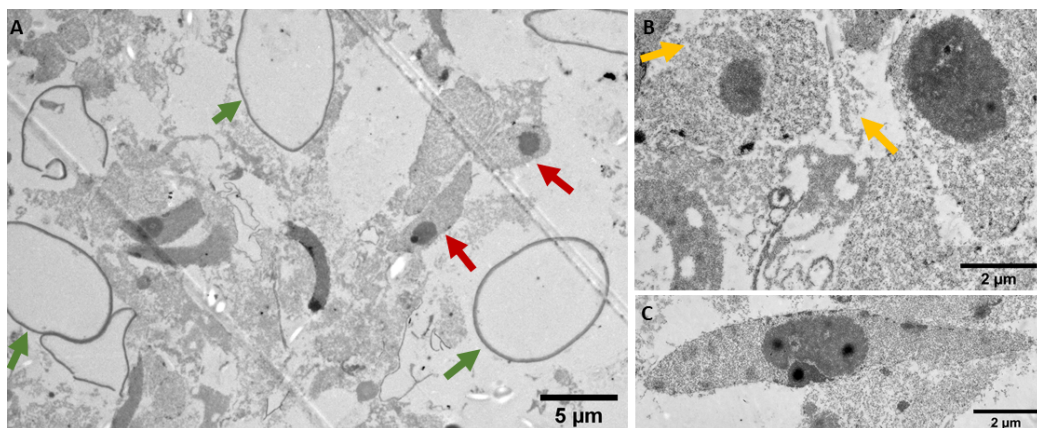


Figure 4.8: A: Overview image of the sample. B, C: Close-up view of nuclei. Red arrows indicate nuclei, green arrows indicate vacuoles, yellow arrows indicate membrane damage.

It was observed that even though the nuclei were purified, the sample contained many vacuoles and other cellular components. Not a single autophago-

some could be found in the sample. This led to the hypothesis that they were destroyed during the sample preparation. This theory was supported by the observed membrane damage of the nuclei, which looked partly dissolved. Different approaches were tried (see Figure 4.9 for detailed information) to improve ultrastructure preservation.

	1	2	3
Pre-fixation	4% PFA 20min	2% PFA + 2% GA 20min	2% PFA + 2% GA 1h in desiccator
Nucleus isolation	Nucleus isolation in 2% PFA + 2.5% GA 1h	Nucleus isolation in 2% PFA + 2% GA 1h	Nucleus isolation in 2% PFA + 2% GA 1h
Washing	Washing	Washing	Washing
Fixation	2% PFA + 2.5% GA overnight	2% PFA + 2% GA overnight	2% PFA + 2% GA overnight

Figure 4.9: Fixation approaches varying in incubation time and concentration of fixatives.

The first approach (see Figure 4.10) with prefixation in 4% PFA for 20 min, nucleus isolation in a mixture of 2% PFA and 2.5% GA, followed by overnight fixation in 2% PFA and 2.5% GA led to non-conclusive results. While some nuclei showed improved ultrastructure, some nuclei appeared even more damaged.

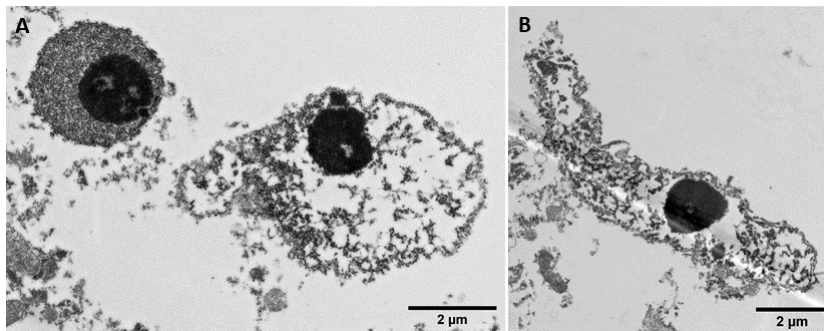


Figure 4.10: A: Isolated nuclei with good (left) and bad (right) ultrastructure next to each other. B: Strongly damaged nucleus.

The second (Figure 4.11A) and third (Figure 4.11B) approach used a mixture of 2% PFA and 2% GA during prefixation, isolation and further fixation. Prefixation of the plants was either for 20 min or for 1 h in a desiccator.

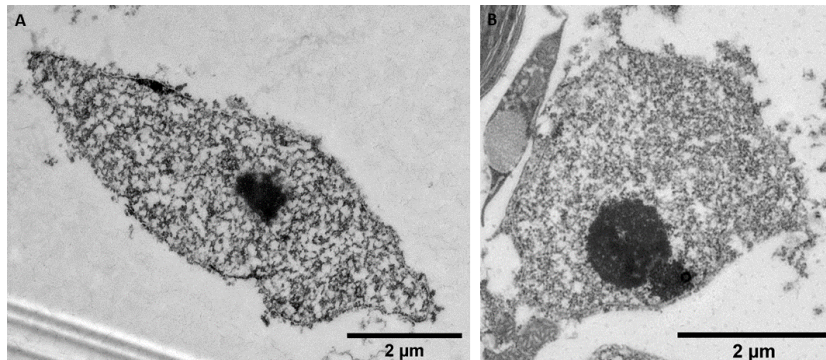


Figure 4.11: A: Isolated nucleus fixed with second approach. B: Isolated nucleus fixed with third approach.

Unfortunately none of the approaches led to satisfying ultrastructure preservation. As before, not a single autophagosome could be found in the samples. This led to the hypothesis that the membranes already get damaged during the nucleus isolation. Nucleus isolation was performed in LB01 lysis buffer, which contains 0.1% Triton X-100. Triton X-100 is a detergent that is regularly used to permeabilize membranes for immunolabeling. While this concentration is common in fluorescence microscopy, it can negatively affect the ultrastructure in TEM. To verify this, nucleus isolation was performed in a LB01 lysis buffer without Triton X-100 (see Figure 4.12). For this sample, the second fixation approach was chosen, because the combination of PFA and GA is common in TEM, and there was no observable improvement when doing the prefixation for a longer time in a desiccator as in the third approach.

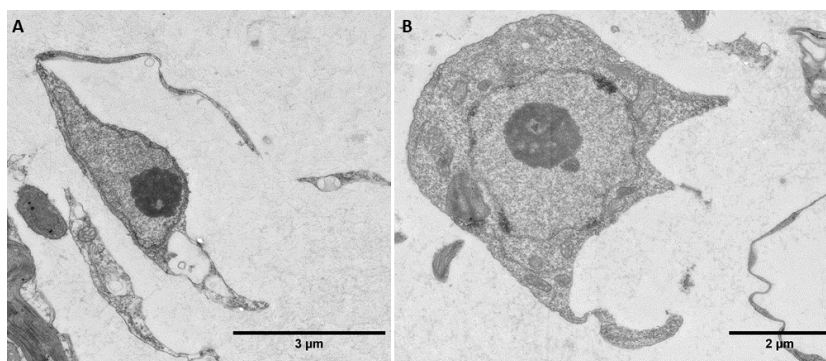


Figure 4.12: A: Well-preserved ultrastructure of an isolated nucleus. B: Well-preserved ultrastructure of a non-isolated nucleus.

As it can be seen in Figure 4.12, the omission of Triton X-100 led indeed to a substantial ultrastructure improvement, but isolation could not be performed

successfully without the permeabilization of the cell wall and cell membrane. Trying different Triton X-100 concentrations is a necessity to find a good compromise. Since TEM sample preparation is extensive and time consuming, this was done in confocal microscopy with the use of a membrane stain.

4.3 Correlation

The combination of chemical fixation and HPF was first tried on isolated nuclei without additional immunolabeling, to see if membrane preservation can generally be improved by freezing. It was difficult to section the HM20 embedded samples, as knife marks appeared inevitably and had stronger impact on the soft resin. Thicker sections were cut (150 nm) to prevent falling apart of the sections and to yield more fluorescently labeled structures inside the sections. Due to the section thickness, samples appeared less sharp under the TEM. Nevertheless, it was possible to find autophagosome candidates in the samples (see Figure 4.13).

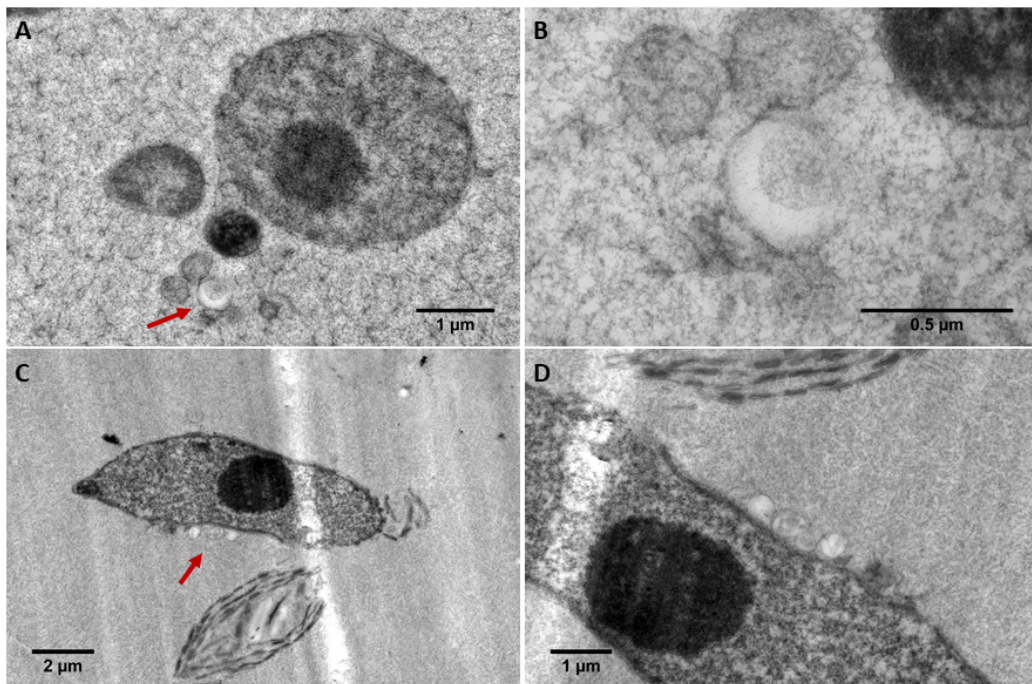


Figure 4.13: A, C: Well-preserved isolated nuclei with autophagosome candidates (indicated by red arrow) with HM20 embedding. B, D: Close-up view of autophagosome candidates.

The sample preparation was repeated with additional immunolabeling. Grids without Formvar coating seemed to be more suitable, because Formvar exhibited noticeable autofluorescence. After observing considerable fluorescent signals in the CLEM microscope, grids were transferred into the TEM. Unfortunately, detected fluorescent regions of interest in the CLEM revealed themselves as fluorescent dirt in the TEM.

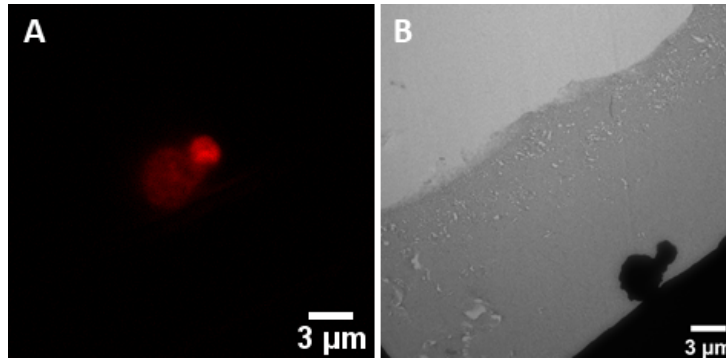


Figure 4.14: A: Red fluorescence in CLEM. B: Same structure in TEM.

An inverted approach was tried, where sections were first searched for nuclei/autophagosomes in TEM and then transferred into the CLEM to confirm this finding via fluorescent signals. This approach was not successful, as fluorescence was gone in areas, which were previously observed via the electron beam due to radiation damage. Additionally, HM20 sections tended to crumble when exposed to the intense electron beam.

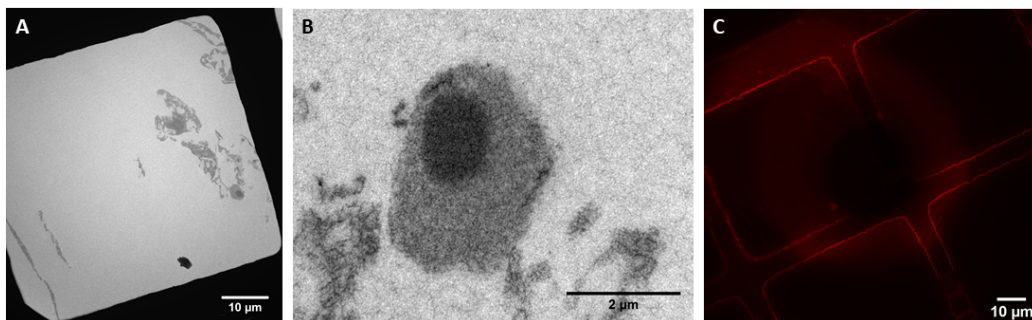


Figure 4.15: Impact of the electron beam on fluorescence signals. 300 nm sections result in blurry appearance. A: Area containing isolated nucleus. B: Close-up view of isolated nucleus. C: Red fluorescence in CLEM.

It seemed that fluorescence of Alexa Fluor 647 was not preserved during TEM sample preparation (despite of optimizing a variety of parameters - compare previous chapters), thus, no dSTORM images of correlative samples were

acquired during this project. However, a correlative set-up was tested in the STORM microscope to see if the sandwich-assembly described in 3.4.2 was feasible with EM grids for future experiments. We were not able to properly focus the sample, because the cover slip would move with the objective. Therefore, the use of a ring holder would be advisable. Even though some fluorescence was detectable, it is arguable if this signal was ATG8. High precision is needed during handling of the sample, because the sections are easily destroyed when disassembling the cover slips.

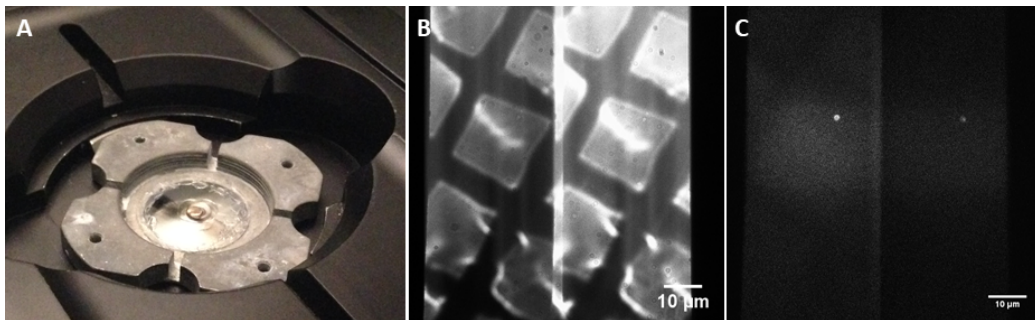


Figure 4.16: A: Sections on EM-grid sandwiched between two circular cover slips. B: Bright-field images (left: blue channel, right: red channel). C: Fluorescence images (left: blue channel, right: red channel).

At the end of the project, three types of fiducial markers were tested. The 0.02 μm and 0.04 μm FluoSpheres were well detectable under fluorescence microscopes, but in TEM they turned out to be irregularly formed and additionally tended to form agglomerations despite previous sonication.

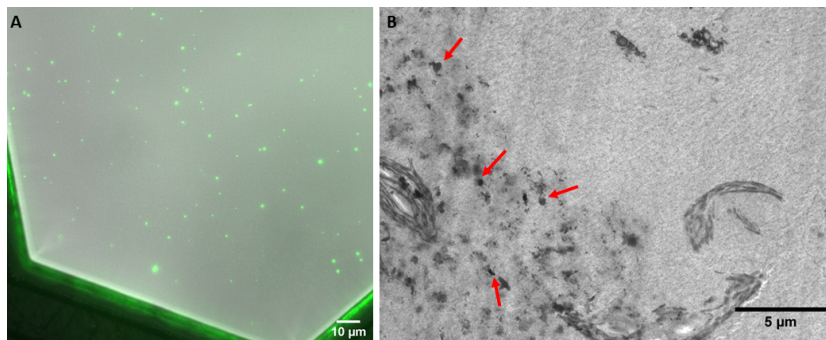


Figure 4.17: Fiducial markers in different modalities. A: FluoSpheres on EM grid observed under CLEM microscope. B: FluoSpheres on HM20 sections containing chloroplasts. Red arrows indicate agglomerated FluoSpheres.

Bigger fiducial markers seemed to be more suitable, since the implemented registration program requires distinctive features. Fluorescence properties of

0.1 μm TetraSpecks were tested, but due to time limitations no TEM images were acquired. It would be necessary to further test fiducial markers in the future to set up a working correlative workflow, which includes registration of the obtained images.

The registration program presented in Listing 3.1 and explained in 3.4.3 Image Registration was scripted and implemented using TEM images of Tobacco Mosaic Viruses provided by A. Walter. The program is semi-automated and worked well on the provided images, resulting in a RMSE of 1.2594 by selecting three fiducial markers in each image. The application on correlative dSTORM and TEM images still needs to be tested.

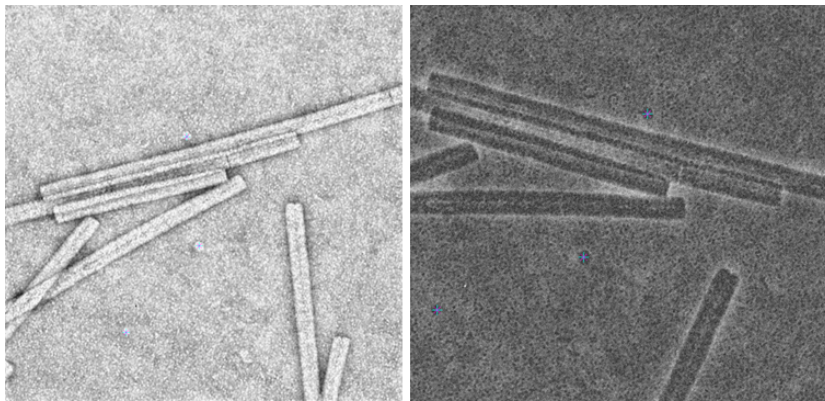


Figure 4.18: Images before registration: Fiducial markers (visible as small circles) were selected with the mouse and marked with a blue cross.

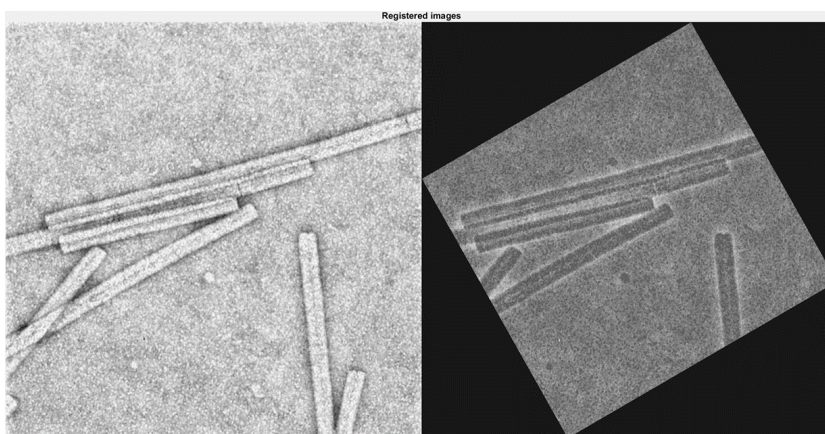


Figure 4.19: Images after registration.

CHAPTER 5

Discussion & Conclusion

This thesis laid the basis for a correlative workflow by implementing sample preparation steps that allow to visualize autophagosomes sequentially with both modalities (dSTORM and TEM) using a sandwich-technique described in 3.4.2. We accomplished to visualize the plant sample with each modality alone and successfully performed embedding in Lowicryl HM20 with preservation of the ultrastructure. We scripted and implemented a MATLAB routine for image registration based on fiducial markers.

During this project we showed that (1) **confocal microscopy** can be readily used to visualize autophagosomes in plants (see 4.1.2). Even though the resolution is limited, autophagosome candidates can be distinguished and DAPI staining of the nucleus facilitates the identification of these autophagosome candidates. Confocal microscopy was especially useful for optimizing sample preparation protocols for dSTORM.

We were able to (2) implement and optimize protocols for **dSTORM** imaging of isolated *Arabidopsis thaliana* nuclei (see 4.1.3). The thickness of the nucleus of a few micrometer combined with the small size of the autophagosome complicated the visualization of autophagosomes in 2D dSTORM. This was solved by cutting (see 3.4.1) and imaging thin sections of the sample as also implemented and needed for imaging with a TEM, thus laying the foundation for an integrated correlative workflow. The correlative workflow was then used to highlight autophagosomes in the sample, which is hardly possible by using dSTORM alone, especially when no additional staining is used. Besides, we succeeded in (3) optimizing **TEM** protocols to visualize intact nuclei with well-preserved ultrastructure (see 4.2). TEM revealed that the nucleus isolation with 0.1% Triton X-100 is not applicable for ultrastructure studies. While nucleus isolation was intended to ease autophagosome detection, it caused many problems, especially in TEM. The permeabilization

process massively damaged membranes. This can result in chromatin escaping from the nuclear envelope, which can be seen as non-overlapping DAPI and Alexa Fluor 647 signals in confocal microscopy. It was difficult to find a working protocol for TEM by using chemical fixation alone and a lot of troubleshooting was necessary to optimize sample preparation. An optimized protocol using a combination of chemical fixation and HPF was identified and yielded first promising results (see 4.3). Overall, it was challenging to find autophagosomes, even when increasing the amount of plants.

We were not able to set up a protocol for correlative dSTORM and TEM which preserved both fluorescence and ultrastructure. Even though the combination of chemical fixation and HPF first led to better result, ultrastructure was not as well preserved when the specimen was additionally labeled with antibodies. It is possible that the sample partially decayed during incubation time due to insufficient fixation. An alternative approach that could be tried to prevent this problem and achieve fluorescence preservation is to directly apply HPF after nucleus isolation and post-label the EM-sections. An example of this workflow was described in 2012 by Fabig et al., who published protocols for correlative immunofluorescence and immunogold labeling on ultrathin sections of samples embedded in Lowicryl K4M [68]. Different resins could also be used to improve fluorescence preservation, when labeling of the sample before embedding is preferred. For the future, it would be helpful to use a ringholder for dSTORM imaging of correlative samples. The adhesion properties of fiducial markers should be tested to see if they continue to stick on the sections after disassembling the sandwich configuration used for dSTORM. The implemented registration program needs to be tested with dSTORM and TEM images. A program using manual point selection is sufficient for the registration of a small data set, but in the long term, a registration software that can automatically detect fiducial markers in dSTORM and TEM images is desired. This requires a lot of data sets, and therefore a working correlative protocol.

In summary, even though we did not create a complete correlative protocol, we were able to (1) implement and optimize imaging and sample preparation protocols for *Arabidopsis thaliana* for the single modalities including confocal, dSTORM and electron microscopy, and to (2) generate comprehensive insights and establish first important working steps towards an advanced correlative workflow of super-resolution CLEM. These findings will be used as the basis for continuing projects.

APPENDIX A

ThunderSTORM Settings

For Figure 4.4, Figure 4.5 and Figure 4.6 the following parameters were used:

Camera setup

Pixel size [nm]	160
Photoelectrons per A/D count	15.3
Base level [A/D counts]	100
EM gain	300

Image filtering

Filter	Wavelet filter (B-Spline)
B-Spline order	3
B-Spline scale	2.0

Approximate localization of molecules

Method	Local maximum
Peak intensity threshold	$a \cdot \text{std}(\text{Wave.F1})$ with $a \in \{1.5, 2\}$
Connectivity	8-neighbourhood

Sub-pixel localization of molecules

Method	PSF: Integrated Gaussian
Fitting radius [px]	$r \in \{2, 3\}$
Fitting method	Weighted Least squares
Initial sigma [px]	1.6
Multi-emitter fitting analysis	disabled

For Figure 4.7 the 'Multi-emitter fitting analysis' was used, which increased computation time significantly and resulted in slightly different parameters:

Approximate localization of molecules

Method	Local maximum
Peak intensity threshold	$a \cdot \text{std}(\text{Wave.F1})$ with $a \in \{2, 2.5\}$
Connectivity	4-neighbourhood

Sub-pixel localization of molecules

Method	PSF: Integrated Gaussian
Fitting radius [px]	3
Fitting method	Weighted Least squares
Initial sigma [px]	1.6
Multi-emitter fitting analysis	enabled
Maximum of molecules per fitting region	5
Model selection threshold (p-value)	1.0E-6
Same intensity for all molecules	disabled
Limit intensity range [photons]	500:2500

APPENDIX B

References

- [1] A. Psenicny: *Korrelative Fluoreszenz- und Elektronenmikroskopie zur Untersuchung von Autophagie*, Technische Universität Wien, 2018.
- [2] S. Michaeli & G. Galili: *Degradation of Organelles or Specific Organelle Components via Selective Autophagy in Plant Cells*, International Journal of Molecular Sciences, Vol. 15, pp. 7624-7638, 2014.
- [3] <http://www.perseus.tufts.edu>
A Greek-English Lexicon, Perseus Digital Library, last visit: November 2018.
- [4] M. Jin et al.: *SnapShot: Selective Autophagy*, Cell, Vol. 152, p. 368, 2013.
- [5] R. S. Marshall & R. D. Vierstra: *Autophagy: The Master of Bulk and Selective Recycling*, Annual Reviews of Plant Biology, pp. 173-208, 2018.
- [6] Y. F. Dagdas et al.: *An effector of the Irish potato famine pathogen antagonizes a host autophagy cargo receptor*, eLife, 2016.
- [7] F. Li & R.D. Vierstra: *Autophagy: a multifaceted intracellular system for bulk and selective recycling*, Trends in Plant Science, Vol. 17, No. 9, p. 531, 2012.
- [8] R. Misri: *Multimodality Imaging*, Molecular Imaging Techniques - New Frontiers: Future Science, pp. 163-178, 2013.
- [9] <http://www.bioimaging-austria.at>
Bioimaging Austria - CMI, last visit: November 2018.

- [10] B. J. Pichler et al. *Multimodal Imaging Approaches: PET/CT and PET/MRI*, Molecular Imaging I. Handbook of Experimental Pharmacology 185/1, Springer-Verlag Berlin Heidelberg, p. 113, 2008.
- [11] G. Antoch et al. *Accuracy of whole-body dualmodality fluorine-18-2-fluoro-2-deoxy-D-glucose positron emission tomography and computed tomography (FDG-PET/CT) for tumor staging in solid tumors: comparison with CT and PET*, Journal of Clinical Oncology, pp. 4357-4368, 2004.
- [12] <http://dan.corlan.net/medline-trend.html>
Alexandru Dan Corlan. Medline trend: automated yearly statistics of PubMed results for any query, last visit: November 2018.
- [13] www.webofknowledge.com
ISI Web of Knowledge, last visit: November 2018.
- [14] D. B. Murphy: *Fundamentals of Light Microscopy and Electronic Imaging*, Wiley-Liss, Inc., 2001.
- [15] <http://crab0.astr.nthu.edu.tw/~hchang/ga1/ch06-01.htm>
High Energy Astrophysics Group: Basic Properties of Optical Telescopes, last visit: February 2019.
- [16] <https://www.microscopyu.com/techniques/super-resolution/the-diffraction-barrier-in-optical-microscopy>
J. S. Silfies et al.: The Diffraction Barrier in Optical Microscopy, last visit: February 2019.
- [17] M. Renz: *Fluorescence Microscopy: A Historical and Technical Perspective*, International Society for Advancement of Cytometry, pp. 767-779, 2013.
- [18] A. Nwaneshiudu et al.: *Introduction to Confocal Microscopy*, Journal of Investigative Dermatology 132, pp. 1-5, 2012.
- [19] J. A. Thorley et al.: *Super-resolution Microscopy: A Comparison of Commercially Available Options*, Fluorescence Microscopy: Super-Resolution and other Novel Techniques pp. 199-212, 2014.
- [20] J. C. Waters et al.: *Concepts in quantitative fluorescence microscopy*, Methods in Cell Biology, Vol. 123, pp. 1-16, 2014.
- [21] J.B. Pawley: *Handbook of Biological Confocal Microscopy*, Springer Science+Business Media, LLC, 2nd Edition, 1995.

- [22] S. Hell & J. Wichmann: *Breaking the diffraction resolution limit stimulated emission: Stimulated-emission-depletion fluorescence microscopy*, Optics Letters, Vol. 19, Issue 11, pp. 780-782, 1994.
- [23] E. Betzig, Eric et al.: *Imaging Intracellular Fluorescent Proteins at Nanometer Resolution*, Science, Vol. 313, Issue 5793, pp. 1642-1645, 2006.
- [24] S. T. Hess, Samuel et al.: *Ultra-High Resolution Imaging by Fluorescence Photoactivation Localization Microscopy*, Biophysical Journal, Vol. 91, Issue 11, pp. 4258-4272, 2006.
- [25] X. Zhuang et al.: *Sub-diffraction-limit imaging by stochastic optical reconstruction microscopy (STORM)*, Nature Methods, Vol. 3, pp. 793-796, 2006.
- [26] M. Baztan et al.: *Advances in super-resolution imaging: applications in biology and medicine*, Microscopy and imaging science: practical approaches to applied research and education, Formatex Research Center, pp. 18-26, 2017.
- [27] J. Tam & D. Merino: *Stochastic optical reconstruction microscopy (STORM) in comparison with stimulated emission depletion (STED) and other imaging methods*, Journal of Neurochemistry 135, pp. 643-658, 2015.
- [28] M. Heilemann et al.: *Subdiffraction-Resolution Fluorescence Imaging with Conventional Fluorescent Probes*, Angewandte Chemie International Edition 47, pp. 6172-6176, 2008.
- [29] M. Sauer: *Localization microscopy coming of age: from concepts to biological impact*, Journal of Cell Science 126, pp. 3505-3513, 2013.
- [30] T. Ha & P. Tinnefeld: *Photophysics of Fluorescent Probes for Single-Molecule Biophysics and Super-Resolution Imaging*, Annual Reviews of Physical Chemistry, pp. 595-617, 2012.
- [31] R. E. Thompson et al.: *Precise Nanometer Localization Analysis for Individual Fluorescent Probes*, Biophysical Journal, Vol. 82, pp. 2775-2788, 2002.
- [32] D. B. Williams & B. C. Carter: *Transmission Electron Microscopy: A Textbook for Materials Science*, Springer US, 2009.

- [33] B. Ayub et al.: *Specimen preparation for electron microscopy: an overview*, Journal of Environment and Life Sciences, Vol. 2, Issue 3, pp. 85-88, 2017.
- [34] H. Pfützner: *Angewandte Biophysik*, SpringerWienNewYork, p. 64, 2003.
- [35] D. Struder et al.: *Electron microscopy of high pressure frozen samples: bridging the gap between cellular ultrastructure and atomic resolution*, Histochemistry and Cell Biology, pp. 877-889, 2008.
- [36] R. Courtland: *Pushing the limits: Technological advances are triggering a revolution in electron microscopy*, Nature, Vol. 563, pp. 462-464, 2018.
- [37] <https://www.leica-microsystems.com/science-lab/how-to-prepare-your-specimen-for-immunofluorescence-microscopy/>
Leica microsystems: How to Prepare Your Specimen for Immunofluorescence Microscopy, last visit: December 2018.
- [38] <https://www.abcam.com/protocols/antibody-structure-and-isotypes>
Abcam: Antibody structure and isotypes, last visit: December 2018.
- [39] <https://www.abcam.com/secondary-antibodies/direct-vs-indirect-immunofluorescence>
Abcam: Direct vs indirect immunofluorescence, last visit: December 2018.
- [40] <https://chromotek.com/about-us/the-alpaca-antibody-advantage/>
Chromotek: The Secret of the Alpaca-Antibody-Advantage, last visit: December 2018.
- [41] <http://www.ablynx.com/technology-innovation/understanding-nanobodies/>
Ablynx: What are nanobodies?, last visit: December 2018.
- [42] B. Q. Huang et al.: *Chemical and Physical Fixation of Cells and Tissues: An Overview*, Plant Microtechniques and Protocols, pp. 23-26, Springer International Publishing Switzerland, 2015.
- [43] <https://www.thermofisher.com/at/en/home/life-science/protein-biology/protein-biology-learning-center/protein-biology-resource-library/pierce-protein-methods/fixation-strategies-formulations.html>
Thermofisher: Fixation Strategies and Formulations Used in IHC Staining, last visit: December 2018.

- [44] I. Hurbain & M. Sachse: *The future is cold: cryo-preparation methods for transmission electron microscopy of cells*, Biology of the Cell, pp. 405-420, 2011.
- [45] H. Kanno et al.: *Supercooling of water to 92°C under pressure*, Science, Vol. 189, pp. 880-881, 1975.
- [46] http://www.zmb.uzh.ch/static/bio407/assets/Bio407_HPF_2013.pdf
Andres Käch: High pressure freezing, last visit: February 2019.
- [47] Y. Su et al.: *Multi-dimensional correlative imaging of subcellular events: combining the strengths of light and electron microscopy*, Biophysics Reviews and Springer, pp. 121-135, 2010.
- [48] Y. S. Bykov et al.: *Correlative light and electron microscopy methods for the study of virus-cell interaction*, FEBS Letters, pp. 1877-1895, 2016.
- [49] P. de Boer et al.: *Correlated light and electron microscopy: ultrastructure lights up!*, Nature Methods, Vol.12, No.6, pp. 503-513, 2015.
- [50] S. Watanabe et al.: *Protein localization in electron micrographs using fluorescence nanoscopy*, Nature Methods, Vol.8, No. 1, pp. 80-84, 2011.
- [51] X. Zhuang et al.: *Correlative Stochastic Optical Reconstruction Microscopy and Electron Microscopy*, Plos One, 2015.
- [52] J. B. A. Maintz & M. A. Viergever: *A survey of medical image registration*, Medical Image Analysis, Vol.2, No 1, pp. 1-36, Oxford University Press, 1998.
- [53] G. Langs: *Medizinische Bildverarbeitung*, Technische Universität Wien, 2017.
- [54] http://www.inf.u-szeged.hu/ssip/2004/proceedings/lectures/Lecture_21.pdf Sven Loncaric: Introduction to Image Registration, last visit: January 2019.
- [55] <https://www.thermofisher.com/at/en/home/life-science/protein-biology/protein-biology-learning-center/protein-biology-resource-library/pierce-protein-methods/amine-reactive-crosslinker-chemistry.html>
Thermofisher: Amine-Reactive Crosslinker Chemistry, last visit: April 2018.

- [56] M. Lysak et al.: *Cytogenetic Analyses of Arabidopsis*, Methods in Molecular Biology Vol. 323: Arabidopsis Protocols Second Edition, pp. 173-186, 2006.
- [57] ImageJ: An open platform for scientific image analysis. Available at <https://imagej.net>
- [58] Python Software Foundation. Python Language Reference, version 3.7.2. Available at <http://www.python.org>
- [59] ThunderSTORM: a comprehensive ImageJ plugin for PALM and STORM data analysis and super-resolution imaging. Available at <https://github.com/zitmen/thunderstorm>
- [60] S. Reipert & G. Wiche: *High-pressure freezing and low-temperature fixation of cell monolayers grown on sapphire coverslips*, Methods in Cell Biology, Vol. 88, pp. 165-180, 2008.
- [61] W. Kukulski et al.: *Precise, Correlated Fluorescence Microscopy and Electron Tomography of Lowicryl Sections Using Fluorescent Fiducial Markers*, Methods in Cell Biology, Vol. 111, pp. 235-257, 2012.
- [62] <https://www.thermofisher.com> Thermofisher, last visit: January 2019.
- [63] The MathWorks, Inc., MATLAB 2016b. Available at: <https://de.mathworks.com/>
- [64] <http://statweb.stanford.edu/~susan/courses/s60/split/node60.html>
Susan Holmes: RMS Error, last visit: January 2019.
- [65] <https://www.abcam.com/protocols/immunoprecipitation-troubleshooting-tips>
Abcam: Immunoprecipitation troubleshooting tips, last visit: January 2019.
- [66] https://www.graphpad.com/guides/prism/7/curve-fitting/index.htm?reg_one_site_specific.htm
GraphPad Software: Equation: One site – Specific binding, last visit: June 2018.
- [67] J. Kuriya et al.: *The Molecules of Life: Physical and Chemical Principles*, Garland Science, p. 536, 2012.

- [68] G. Fabig et al.: *Labeling of Ultrathin Resin Sections for Correlative Light and Electron Microscopy*, Methods in Cell Biology, Vol. 111, pp. 75-93, 2012.